

Formation of SiC Grains in Pulsation–Enhanced Dust–Driven Wind around Carbon–Rich Asymptotic Giant Branch Stars

Yuki Yasuda and Takashi Kozasa

*Department of CosmoSciences, Graduate School of Science, Hokkaido University, Sapporo
060–0810, Japan*

yuki@antares-a.sci.hokudai.ac.jp

ABSTRACT

We investigate the formation of silicon carbide (SiC) grains in the framework of dust–driven wind around pulsating carbon–rich Asymptotic Giant Branch (C–rich AGB) stars in order to reveal not only the amount but also the size distribution. Two cases are considered for the nucleation process; one is the LTE case where the vibration temperature of SiC clusters T_v is equal to the gas temperature as usual, and another is the non–LTE case in which T_v is assumed to be the same as the temperature of small SiC grains. The results of hydrodynamical calculations for a model with stellar parameters of mass $M_*=1.0 M_\odot$, luminosity $L_*=10^4 L_\odot$, effective temperature $T_{\text{eff}}=2600$ K, C/O ratio=1.4, and pulsation period $P=650$ days show the followings: In the LTE case, SiC grains condense in accelerated outflowing gas after the formation of carbon grains and the resulting averaged mass ratio of SiC to carbon grains of $\sim 10^{-8}$ is too small to reproduce the value of 0.01–0.3 inferred from the radiative transfer models. On the other hand, in the non–LTE case, the formation region of SiC grains is inner than and/or almost identical to that of carbon grains due to the so–called inverse greenhouse effect. The mass ratio of SiC to carbon grains averaged at the outer boundary ranges from 0.098 to 0.23 for the sticking probability $\alpha_s=0.1$ –1.0. The size distributions with the peak at ~ 0.2 – $0.3 \mu\text{m}$ in radius cover the range of size derived from the analysis of presolar SiC grains. Thus the difference between temperatures of small cluster and gas plays a crucial role in the formation process of SiC grains around C–rich AGB stars, and this aspect should be explored for the formation process of dust grains in astrophysical environments.

Subject headings: circumstellar matter; dust, extinction; stars: AGB and post–AGB; stars: winds, outflows

1. INTRODUCTION

Presolar silicon carbide (SiC) is the abundant and well studied dust species among presolar grains extracted from meteorites. Based on the isotopic compositions of C, N, Si and Al, presolar

SiC grains are classified into six categories named “mainstream”, A, B, X, Y and Z grains (e.g., see Ott 2010 for a review). Among them, the mainstream grains populating about 90 % of presolar SiC grains have been considered to be originated in carbon-rich Asymptotic Giant Branch (C-rich AGB) stars from the isotopic compositions of C, N, and Si (Zinner et al. 1987; Hoppe et al. 1994) and the s-process signatures in the noble gases as well as in the heavy elements (Hoppe & Ott 1997). Amari et al. (1994) have reported that SiC grains extracted from the Murchison meteorite have a log-normal distribution with the peak at $\sim 0.4 \mu\text{m}$ in diameter, and 70 % of them by number are in the grains whose diameter ranges from 0.3 to $0.7 \mu\text{m}$ (Daulton et al. 2003). Although it was reported that SiC grains are more fine grained in other meteorites than in Murchison (see Russell et al. 1997), a significant fraction of presolar SiC grains are larger than $0.3 \mu\text{m}$ in diameter (see Hoppe & Zinner 2000). Thus, submicron-sized SiC grains are expected to form around C-rich AGB stars. The presence of SiC grains in C-rich AGB stars was confirmed from the emission feature around $11.3 \mu\text{m}$ (Hackwell 1972; Treffers & Cohen 1974; Goebel et al. 1980), prior to the discovery of presolar SiC grains (Bernatowicz et al. 1987). Also, the absorption feature attributed to SiC grains was observed in several extreme carbon stars (Jones et al. 1978; Speck et al. 1997, 2009). The radiative transfer models fitting the observed spectral energy distributions (SEDs) including the spectral feature attributed to SiC grains have estimated the mass ratio of SiC to carbon grains to be in the range of 0.01–0.3 (Lorenz-Martins & Lefèvre 1993, 1994; Blanco et al. 1994, 1998; Groenewegen 1995; Groenewegen et al. 1998). The variation of the mass ratio of SiC to carbon derived from the radiative transfer models arises from the grain models used, and the value could be also influenced by the optical constants of SiC used in the radiative transfer models (see the discussion in Section 6).

Although the isotopic signatures of presolar SiC grains and the observed spectral feature around $11.3 \mu\text{m}$ support the formation of SiC grains in circumstellar envelopes of C-rich AGB stars, the formation process as well as the formation conditions remain unknown and debatable: Thermodynamic equilibrium calculations have been applied to investigate the formation condition of dust grains in C-rich AGB stars (e.g. Lodders & Fegley 1995), and the calculations have claimed that high gas pressure ($0.3\text{--}300 \text{ dyne cm}^{-2}$) and low C/O ratio ($1.0 < \text{C/O} \lesssim 1.1$) is necessary for reproducing the condensation sequence of presolar TiC, graphite, and SiC grains in this order inferred from the presence of graphitic spherules containing a TiC core (Sharp & Wasserburg 1995; Daulton et al. 2003). On the other hand, McCabe (1982) suggested the formation of SiC grains earlier than carbon grains, considering the inverse greenhouse effect that the temperature of SiC grains which is transparent in the optical to near infrared (NIR) region (Spitzer 1959; Hofmeister et al. 2009) is lower than the temperature of carbon grains in circumstellar envelopes of C-rich AGB stars. In addition, the interferometric observation of IRC+10216 at $11 \mu\text{m}$ has suggested the presence of dust species more transparent than carbon grains in the inner circumstellar envelope close to the photosphere (Danchi et al. 1990). Although thermodynamic equilibrium calculations can tell us the physical conditions in which a condensate exists stably, the calculations as well as the astronomical observations provide directly no information on the number and size of grains that are essential to clarify the physical conditions prevailing in the formation sites of grains and the

physical and chemical processing suffering in the interstellar space. Also, it should be pointed out here that the C/O ratio in C-rich AGB stars is not restricted to be less than 1.1, and tends to increase with decreasing the effective temperature T_{eff} ; the low C/O ratio observed in stars with $T_{\text{eff}} \lesssim 2500$ K is considered to be caused by the neglect of formation of dust in the model atmosphere (Bergeat et al. 2002; Bergeat & Chevallier 2005).

So far dust formation around C-rich AGB stars has been investigated in the framework of pulsation-enhanced dust-driven wind models since the study by Fleischer et al. (1992), and it has been believed that the hydrodynamical models including only the formation of carbon grains well reproduce the observed dynamical behavior of C-rich AGB stars whose mass loss rates exceed $10^{-6} M_{\odot} \text{ yr}^{-1}$ (e.g., Winters et al. 1994, 1997; Nowotny et al. 2005). However, the formation of SiC grains has not yet pursued in the hydrodynamical models. On the other hand, formation of a variety of dust species including SiC grains has been studied in the steady state dust-driven wind models around AGB stars in order to investigate the evolution of dust in the interstellar space (see Ferrarotti and Gail 2006; Zhukovska et al. 2008). However, in the models, the number of seed nuclei is assumed in the formation process. Although the models may predict the mass of dust species supplied from AGB stars, no information is available for the size distribution. Taking into account the nucleation process and including the so-called inverse greenhouse effect, Kozasa et al. (1996) have investigated the formation of SiC grains in an outflowing gas with constant velocity around C-rich AGB stars and shown that SiC grains condense prior to carbon grains for the mass-loss rate smaller than $\sim 1.5 \times 10^{-5} M_{\odot} \text{ yr}^{-1}$; otherwise composite grains consisting of carbon and SiC form. The calculated radius of $\sim 0.01 \mu\text{m}$ is too small to reproduce the size of presolar SiC grains and the proposed grains consisting of a SiC core and a carbon mantle have not been discovered except for one in presolar grains (Croat et al. 2010). Thus the investigation of formation of SiC grains in a more realistic hydrodynamical model remains an important subject to be explored which will reveal the formation process and condition around C-rich AGB stars. The knowledge of not only the amount but also the size distribution of dust grains is crucial for investigating the role of dust in the universe as shown by Yamasawa et al. (2011). In particular, the size distribution of SiC grains formed around C-rich AGB stars is vital to get insight into the evolution and processing during the journey from the formation sites to the incorporation into meteorites from the analysis of presolar SiC grains.

In this paper, we aim at exploring the formation process of SiC grains and investigating the amount as well as the size distribution in the framework of pulsation-enhanced dust-driven wind from C-rich AGB stars. We develop the hydrodynamical model including formation of carbon and SiC grains as well as a non-grey radiative transfer. The formulation by Gauger et al. (1990) is applied for the nucleation and growth processes of carbon grains¹. We assert that SiC

¹In the formulation it is assumed that carbon grains nucleate and grow homogeneously. The recent analysis of presolar graphites (Croat et al. 2005) revealed that about 40 % of the carbide-containing graphites have a carbide core at their center. This implies that at least more than 60 % of presolar graphites nucleate and grow homogeneously.

grains nucleate and grow homogeneously starting from SiC molecule because all presolar SiC grains whose internal structure has thus far been analyzed do not contain any seed nuclei at their centers (Stroud & Bernatowicz 2005). Furthermore there is no evidence in presolar graphite grains for a SiC seed nuclei except for one grain (Croat et al. 2010). The two cases are considered for the formation process of SiC grains; one is the LTE case where the vibration temperature T_v of SiC cluster is the same as the gas temperature as usual. Another is the non-LTE case taking into account the inverse greenhouse effect on the formation, in which T_v is assumed to be the same as the temperature of small SiC grains. We will show that the mass ratio of SiC to carbon grains and the radius of SiC grains are at most 10^{-6} and $0.1 \mu\text{m}$, respectively, in the LTE case, while the mass ratio ranges from 0.098 to 0.23 and the typical radius ranges from 0.2 to $0.6 \mu\text{m}$ for the sticking probability α_s of 0.1–1.0 in the non-LTE case.

This paper is organized as follows; The chemical reactions and gas species relevant to the formation of SiC grains are examined and the formation process of SiC grains is formulated in Section 2, and the numerical scheme for calculation of grain formation is presented in Section 3, including the method for tracing the size distribution. Section 4 describes the hydrodynamical model and the modeling procedure for pulsation-enhanced dust-driven wind model including dust formation and radiative transfer. The results of calculations are presented in Section 5 and are discussed in Section 6. Summary is presented in Section 7.

2. FORMATION PROCESS OF SiC GRAINS

In the hydrodynamical models of pulsation-enhanced dust-driven wind from C-rich AGB stars so far developed since the work of Fleischer et al. (1992), the formation of carbon grains has been processed according to the recipe developed by Gauger et al. (1990); the abundances of gas species responsible for the nucleation and growth of carbon grains are assumed to be in chemical equilibrium in the gas whose elemental abundance is solar except for carbon. In the recipe based on Gail & Sedlmayr (1988), the formation of clusters with number of constituent molecules (size) up to $n_{\text{out}}=1000$ is evaluated from the steady-state nucleation rate, and the growth and evaporation of grains with size $n \geq n_{\text{out}}$ is treated as macroscopic grains. The formation of carbon grains are considered to proceed through the two body reactions of C_2H_2 and C_2H molecules with carbon clusters, starting from atomic carbon or diatomic carbon molecule.

In this section, we shall explore the formation process of SiC grains around C-rich AGB stars, following the formulation for the formation of carbon grains (Gail & Sedlmayr 1988; Gauger et al. 1990). First we examine the gas species responsible for the nucleation and the growth processes of SiC grains from chemical equilibrium calculations. In the same way as the formation of carbon grains, we consider that the nucleation process proceeds through the two body reactions of cluster with gas species, starting from the molecules whose stoichiometric composition is the same as SiC grains. On the other hand, we allow three or more body reactions on the surface for the growth process. Then, the basic equations describing the nucleation and growth processes of SiC grains

are presented.

2.1. Si-bearing gas species in dust formation region

Figure 1 shows the temperature dependence of relative abundances of Si-bearing molecules (left) and C-bearing molecules (right) in chemical equilibrium in the gas with the density $\rho = 10^{-13} \text{ g cm}^{-3}$ and $\text{C/O} = 1.4$, which is calculated by the method of the minimization of the Gibbs free energies. The elemental abundances except for carbon are taken from Allen (1973), and the thermodynamic data are taken from Chase et al. (1985) except for C_2H_2 (Cherchneff et al. 1992), SiC_3 , SiC_4 , SiC_5 , Si_2C_2 , Si_2C_3 , Si_2C_4 , Si_3C , Si_3C_2 , Si_3C_3 , Si_4C , Si_4C_2 , and Si_5C (Deng et al. 2008). We can see that, as the starting molecules for the formation of SiC grains, SiC is most abundant in the region whose gas temperature is higher than 1350 K, while Si_2C_2 molecule is abundant in the lower temperature region. Among Si-bearing molecules that are considered to be candidate reactants in the growth process of SiC grains, Si, SiC_2 , and SiS molecules are abundant in the overall range of gas temperature presented in Figure 1, and Si_2C is also abundant in the low temperature region of $T < 1100 \text{ K}$. As shown in the right panel, hydrocarbon molecules such as C_2H_2 or C_2H are expected to be reactants participating in the growth process on the surface of SiC grains unless these molecules are heavily depleted by the formation of carbon grains.

2.2. Nucleation process of SiC grains

Including the starting molecules SiC and Si_2C_2 for the nucleation process, the candidate reactants for the two body reaction in the nucleation process are confined to twelve Si-bearing molecules: SiC, SiC_2 , SiC_3 , SiC_4 , Si_2C , Si_2C_2 , Si_2C_3 , Si_3C , Si_3C_2 , Si_4C , Si_4C_2 , and Si_5C . We shall exclude the gas species with which the reaction for formation of SiC clusters is endothermic. Table 1 presents the reaction enthalpies ΔH° of the twelve candidates for the formation of Si_2C_2 and Si_3C_3 at 1000 and 1500 K. The molecules SiC_2 , SiC_3 , SiC_4 , Si_2C , Si_2C_3 , Si_3C , Si_4C , and Si_5C are excluded from the candidates since the reactions are endothermic. The reaction enthalpies for the formation of SiC clusters with $n > 3$ for which no thermodynamic data is available are replaced with those for the formation of solid SiC, and the values at 1000 and 1500 K are listed in Table 2 where the thermodynamic data of $\beta\text{-SiC}^2$ is used in the calculations. The molecules SiC_2 and Si_5C are excluded because of the endothermic reactions. Among the remaining candidates, as the reactants in the nucleation process of SiC grains, we adopt SiC and Si_2C_2 since these molecules are much more abundant than the others in the temperature region of interest to us as shown in Figure 1 (left).

² Presolar SiC grains so far analyzed show only two polytypic forms (Daulton et al. 2003): $\beta\text{-SiC}$ (79.4 % by number), $\alpha\text{-SiC}$ (2.7 %), and the intergrowths of these two forms (17.1 %). Note that the difference of thermodynamic data between $\alpha\text{-SiC}$ and $\beta\text{-SiC}$ does not affect the results of calculations presented in this paper.

We discard the nucleation process starting from the two body reaction between Si_2C_2 molecules since Si_2C_2 is relatively stable and without the thermodynamic data of Si_4C_4 it is difficult to judge whether the reaction for the formation of Si_4C_4 proceeds or not. Thus we consider the following two reactions in the nucleation process of SiC grains:



where $n \geq 1$, and note that we take SiC as the starting molecule for the nucleation process of SiC grains. We shall discuss the effect of the nucleation process starting from the two body reaction of Si_2C_2 molecules in Section 6.

In the nucleation process, clusters grow through the attachment of reactant and the growth rate depends on the number density and kinetic temperature of the reactants. On the other hand, clusters decay through the detachment of reactant molecules, and the decay rate depends on the vibration states of the cluster (Gail & Sedlmayr 1988). As pointed out by Kozasa et al. (1996), in the dust formation region around C-rich AGB stars, the vibration temperature of SiC cluster T_v is not always the same as the kinetic temperature of gas T due to the low gas density and strong radiation field. The principle of detailed balance being applied, the decay rate can be related with the growth rate by considering a hypothetical situation in which the cluster is in a local thermal equilibrium with the ambient gas whose temperature is T_v . Then, under the assumption that T_v is independent of the size of cluster, the steady-state nucleation rate J_S^i for the reaction with $(\text{SiC})_i$ is given by

$$J_S^i = 4\pi\alpha_s^i a_0^2 n_{\text{SiC}} n_i \sqrt{\frac{k_B T}{2\pi m_i}} \times \left[1 + \sum_{k=1}^{N_x} \frac{\exp\left\{4\pi a_0^2 (ik)^{2/3} \sigma_{ik+1} / k_B T_v\right\}}{(ik+1)^{2/3} \left\{S_i(T_v, P_i) \sqrt{T/T_v}\right\}^k} \right]^{-1} \quad (3)$$

where $i=1$ (2) denotes the reaction (1) (the reaction (2)) and the quantities related with the reactant SiC (Si_2C_2) molecule, a_0 is the hypothetical radius of a monomer in the bulk phase, n_{SiC} the number density of starting molecule SiC. The number density, sticking probability, mass, and partial pressure of the i -th reactant is represented by n_i , α_s^i , m_i , and P_i , respectively. The Boltzmann constant is k_B , $N_x = \lfloor (n_{\text{out}} - 2)/i \rfloor$ with the floor function $\lfloor x \rfloor$, and the surface tension of the cluster of size n σ_n . The supersaturation ratio $S_i(T_v, P_i)$ is given by

$$\ln S_i(T_v, P_i) = -\frac{\Delta G_i^0}{k_B T_v} + \ln \frac{P_i}{P_0}. \quad (4)$$

where P_0 is the standard pressure. In the above equation, ΔG_i^0 is the Gibbs free energy for the formation of bulk SiC from the i -th reactant in the standard pressure, and the temperature dependence of $\Delta G_i^0/k_B T_v$ is evaluated from the least-squares fitting given by

$$\frac{\Delta G_i^0}{k_B T_v} = \alpha_i + \beta_i \ln T_v + \frac{\gamma_i}{T_v^{0.5}} + \frac{\delta_i}{T_v} + \frac{\eta_i}{T_v^2} + \frac{\epsilon_i}{T_v^3}. \quad (5)$$

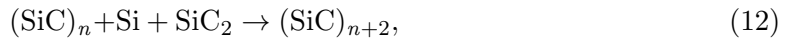
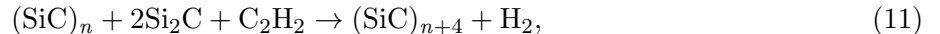
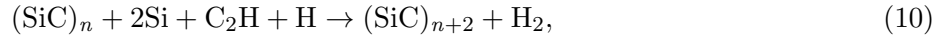
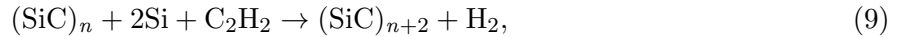
whose form is based on a polynomial expression of heat capacity at the constant pressure (Berman & Brown 1985). The coefficients α_i , β_i , γ_i , δ_i , η_i and ϵ_i are given in Table 3. In the calculations, we adopt $a_0=1.71\times 10^{-8}$ cm which is evaluated from the bulk density of solid SiC ($\rho=3.16$ g cm $^{-3}$) taken from the CRC hand book (Lide 2003). The values of the sticking probabilities of SiC and Si $_2$ C $_2$ molecules on the SiC cluster are unknown and are assumed to be unity. The surface tension σ_n of SiC cluster with size $n=2$ or 3 is directly evaluated from the following definition of surface tension of n -mer

$$4\pi a_0^2(n-1)^{\frac{2}{3}}\sigma_n = \dot{g}(n) - \dot{g}(1) - (n-1)\dot{g}_s \quad (6)$$

where $\dot{g}(n)$ and \dot{g}_s are the Gibbs free energies of n -mer in gas phase and the monomer in bulk phase in the standard state, respectively. On the other hand, we adopt the bulk value of $\sigma=840$ erg cm $^{-2}$ measured by Allen & Kingery (1959) as the surface tension of SiC clusters with size $n > 3$.

2.3. Growth of SiC grains

We allow three or more body reactions for the growth of SiC grains in addition to the two body reactions for the nucleation. As shown in Figure 1, the abundant Si- and C-bearing molecules expected to be the reactants for the grain growth are Si, SiC $_2$, Si $_2$ C, C, C $_2$ H $_2$, and C $_2$ H, except for CO and SiS which are stable against the chemical reactions. Then we select the following exothermic reactions;



where $n > n_{\text{out}}=1000$; the reaction enthalpies at 1000 K are -1265, -1739, -1572, -1206, and -1240 kJ mol $^{-1}$ for the chemical reactions from (9) to (13) in this order.

Except for the two body reactions, it is assumed that each of the chemical reactions proceeds through the attachment of a key species which is defined as the species of the least collision frequencies among the reactants and is considered to control the kinetics of growth process (Kozasa & Hasegawa 1987; Hasegawa & Kozasa 1988). Then, the time evolution of the size of dust grains with radius a is given by

$$\frac{d}{dt} \left(\frac{a}{a_0} \right) = \frac{1}{3\tau_{\text{net}}} \quad (14)$$

where the size-independent net time scale of grain growth τ_{net} (Gauger et al. 1990) is the sum of the net time scales for the reactions from (7) to (13) and is written as follows:

$$\frac{1}{\tau_{\text{net}}} = \sum_{i=1}^2 \frac{1}{\tau_{\text{net}}^i} + \sum_{n=9}^{13} \frac{1}{\tau_{\text{net}}^{\text{C},n}}. \quad (15)$$

In the above equation, τ_{net}^i ($i=1,2$) is the net time scale of grain growth by the two body reaction with $(\text{SiC})_i$ molecule and given by

$$\frac{1}{\tau_{\text{net}}^i} = i4\pi a_0^2 \alpha_s^i \sqrt{\frac{k_B T}{2\pi m_i}} \left(n_i - \frac{P_{\text{ev}}}{k_B \sqrt{TT_v}} \right), \quad (16)$$

and $\tau_{\text{net}}^{\text{C},n}$ ($n=9$ to 13) is the net time scale of grain growth for each of the chemical reactions from (9) to (13) and is given in the same form of equation (16) by replacing α_s^i , m_i and n_i with those for the key species. In equation (16), P_{ev} represents the vapor pressure for the key species in the reaction; for example, in the reactions (9) and (10), the vapor pressure of Si atom is assumed to be the same as that for the reaction: $(\text{SiC})_s \rightarrow \text{Si} + \text{C}$. In the reaction (11), the vapor pressure of Si_2C molecule is assumed to be the same as that for the reaction: $2(\text{SiC})_s \rightarrow \text{Si}_2\text{C} + \text{C}$. In the calculations, the sticking probability α_s is assumed to be unity for all reactions.

3. NUMERICAL SCHEME FOR GRAIN FORMATION

The number densities of the gas species responsible for the formation process of carbon and SiC grains in the pulsation-enhanced dust-driven wind from C-rich AGB stars are evaluated from the chemical equilibrium calculations for given gas density and temperature coupled with the hydrodynamical calculation. We include 4 atoms (H, C, Si, S) and 14 molecules (H_2 , C_2 , C_3 , C_2H , C_2H_2 , SiH, SH, H_2S , SiC, SiC_2 , Si_2C , Si_2C_2 , CS, SiS) in the chemical equilibrium calculations, and the abundances of elements except for carbon are taken from the table of Allen (1973). We employ the formulation presented in Section 2 for the formation process of SiC grains, while the formulation by Gauger et al. (1990) is applied for the formation of carbon grains. As mentioned before, the sticking probability α_s for all reactions at nucleation and growth of SiC grains is assumed to be unity in the calculations, whose effect on the results of calculations is discussed in Section 6.

The number density and size of grains as well as the fraction of condensible molecules locked into grains are evaluated by taking the j -th moment of the size distribution of grains per H-element \hat{K}_j defined as

$$\hat{K}_j = \sum_{n=n_{\text{out}}}^{\infty} N^{\frac{j}{3}} \frac{f(n,t)}{n_{\langle \text{H} \rangle}} \quad (17)$$

where $f(n,t)$ is the number density of grains with the size n at time t and $n_{\langle \text{H} \rangle} = n_{\text{H}} + 2n_{\text{H}_2}$. Normally, the moments are calculated by reducing to the simultaneous differential equations (Gail & Sedlmayr

1988). The time variation of gas (grain) temperature is not always monotonic and rather complicated in the pulsation–enhanced dust–driven winds. In the case that the formed grains are being lost by the destruction due to evaporation at time t , the extinction term is included in the differential equations by using the number density of grains with the minimum size $f(n_{\text{out}}, t)$ which has to be derived by tracing the size distribution. Therefore, solving the differential equations must be compensated with the evaluation of the size distribution of grains with a limited number of size bins in the hydrodynamical simulations (Fleischer 1994).

Thus, in this paper, we calculate the moments by employing the finite and adaptive size grids rather than solving a set of the simultaneous differential equations. Each of the size bins is comoved in size space (Krüger et al. 1995; Woitke & Niccolini 2005). The i -th size bin is characterized by the number of grains per H–element $\hat{w}(i)$ in the size interval with lower limit $a_{i,\text{min}}$ and upper limit $a_{i,\text{max}}$. The lower and upper limits are calculated by integrating equation (14). When the net time scale τ_{net} is positive, the number of grains per H–element in the lowest size bin $\hat{w}(I)$ where I is the total number of size bins is given by integrating the equation

$$\frac{d\hat{w}(I)}{dt} = \frac{J_{\text{S}}}{n_{\langle\text{H}\rangle}}. \quad (18)$$

When the net time scale τ_{net} is negative, with the destruction rate of grains J_{des} estimated by

$$J_{\text{des}} = -\frac{da}{dt} \frac{\hat{w}(I)n_{\langle\text{H}\rangle}}{a_{I,\text{upper}} - a_{\text{lowest}}} \quad (19)$$

where $a_{\text{lowest}} = a_0 n_{\text{out}}^{1/3}$, $\hat{w}(I)$ is derived by integrating the equation

$$\frac{d\hat{w}(I)}{dt} = -\frac{J_{\text{des}}}{n_{\langle\text{H}\rangle}}. \quad (20)$$

According to Woitke & Niccolini (2005), the discrete moment \hat{K}_j^{discr} is evaluated by

$$\hat{K}_j^{\text{discr}} = \frac{1}{(j+1)a_0^j} \left\{ \sum_{i=1}^{I-1} \hat{w}(i) \sum_{k=0}^j a_{i,\text{min}}^k a_{i,\text{max}}^{j-k} + \hat{w}(I) \sum_{k=0}^j a_{\text{lowest}}^k a_{I,\text{max}}^{j-k} \right\} \quad (21)$$

for $j=0$ to 3. The 0–th moment \hat{K}_0^{discr} and the 3rd moment \hat{K}_3^{discr} give the number of grains per H–element and the number of condensible molecules incorporated into grains per H–element, respectively. The volume equivalent radius of grains $\langle a \rangle$ at a time is defined by $\langle a \rangle = a_0 (\hat{K}_3^{\text{discr}} / \hat{K}_0^{\text{discr}})^{1/3}$.

4. THE MODEL

4.1. Hydrodynamics

The basic equations for the time–dependent spherically symmetric hydrodynamical model are written in standard finite difference form and solved by explicit integration along the lines of

difference scheme given by Richtmyer & Morton (1967). This modeling method has been adopted by Berlin group (e.g., Fleischer et al. 1992; Winters et al. 2000; Helling et al. 2000; Dreyer et al. 2011). Actually, this method is time-consuming since the time steps are restricted by the Courant–Friedrichs–Levy (CFL) stability condition (see Höfner et al. 1996). However, since the advection term drops out from the equation of motion in Lagrangian coordinate, we can easily trace the size distribution of grains which is one of main subjects of this study.

The continuity equation representing the conservation of mass is replaced with the definition of gas velocity v given by

$$\frac{\partial r}{\partial t} = v \quad (22)$$

where r is the radial position of the Lagrangian mass element at a time t . Under the assumption of position coupling between gas and grains, the equation of motion is described as

$$\frac{\partial v}{\partial t} = -\frac{1}{\rho} \frac{\partial p}{\partial r} - \frac{GM(r)}{r^2} (1 - \alpha) \quad (23)$$

where p is the thermal gas pressure, ρ is the gas density, G is the gravitational constant, and $M(r)$ is the mass inside a radius r . In the above equation, α is the ratio of radiation pressure force to gravity and expressed as

$$\alpha = \frac{\kappa_{\text{pr}} L_*}{4\pi c GM(r)} \quad (24)$$

where κ_{pr} is the sum of the flux weighted mean of mass radiation pressure coefficient for gas $\kappa_{\text{pr}}^{\text{gas}}$ and that for dust $\kappa_{\text{pr}}^{\text{dust}}$, L_* the luminosity, and c the speed of light. The mass inside a radius r in the above equations is replaced with the stellar mass M_* because the mass contained in the circumstellar envelope is small compared to the stellar mass during the calculations presented in this paper. In the calculations, we adopt the constant gas opacity of $\kappa_{\text{g}} = 2 \times 10^{-4} \text{ cm}^2 \text{ g}^{-1}$ (Bowen 1988). Following the previous works for hydrodynamic models of dust-driven wind solved with frequency dependent radiative transfer calculation (Höfner et al. 2003; Woitke 2006; Mattsson et al. 2010), we evaluate the dust opacity $\kappa_{\lambda}^{\text{dust}}$ at a wavelength λ in the Rayleigh approximation. The optical constants of carbon and SiC grains used in the calculation are taken from Draine (1985)³ and Choyke & Palik (1985), respectively. The radiation field in the circumstellar envelope is derived from the frequency-dependent radiative transfer calculation using the variable Eddington factor method under the assumption of radiative equilibrium. Then, the gas temperature T_{gas} is given by

$$\int_0^{\infty} \kappa_{\lambda, \text{abs}}^{\text{gas}} J_{\lambda} d\lambda = \int_0^{\infty} \kappa_{\lambda, \text{abs}}^{\text{gas}} B_{\lambda}(T_{\text{gas}}) d\lambda \quad (25)$$

³The Rosseland mean and Planck mean absorption coefficients calculated by the optical constants of graphite (Draine 1985) are almost the same as those calculated by the optical constants of amorphous carbon (Rouleau & Martin 1991) used in the recent hydrodynamical calculations (e.g., Höfner et al. 2003; Mattsson et al. 2010). Thus, the difference in the optical constants does not so much affect the results of calculations presented in this paper.

where the subscript “abs” refers to absorption, J_λ is the mean intensity and $B_\lambda(T_{\text{gas}})$ the Planck function. The temperature of i -th grain species $T_{\text{dust},i}$ is given by

$$\int_0^\infty \kappa_{\lambda,\text{abs}}^{\text{dust},i} J_\lambda d\lambda = \int_0^\infty \kappa_{\lambda,\text{abs}}^{\text{dust},i} B_\lambda(T_{\text{dust},i}) d\lambda. \quad (26)$$

4.2. Vibration temperature of SiC cluster

According to the hydrodynamical models developed so far for dust-driven wind from C-rich AGB stars (Fleischer et al. 1992; Höfner et al. 1995), the vibration temperature of carbon cluster is set to be equal to the gas temperature as usual. On the other hand, in order to investigate the influence of the inverse greenhouse effect suggested by McCabe (1982) for the formation of SiC grains, we consider the two cases for the vibration temperature of SiC cluster: One is the case that the vibration temperature of SiC cluster is the same as the gas temperature and that is referred to as the LTE case hereafter. Another is the non-LTE case where the vibration temperature is assumed to be the same as the temperature of small SiC grains (Kozasa et al. 1996). Assuming that the gas species mainly consisting of H, H₂, and He accommodate with grains completely upon colliding, and placing a small SiC grain hypothetically at a position in the gas flow, we derive the vibration temperature of SiC cluster T_v by balancing the heating with the cooling through the interaction with radiation and gas as follows;

$$\int \pi Q_{\lambda,\text{abs}}^{\text{SiC}}(a_{\text{cl}}) [J_\lambda - B_\lambda(T_v)] d\lambda = \sum_j n_{\text{gas},j} \left(\frac{k_B T_v}{2\pi m_j} \right)^{\frac{1}{2}} (C_{V,j} + \frac{1}{2} k_B) \left(T_v - T_{\text{gas}} \sqrt{\frac{T_{\text{gas}}}{T_v}} \right) \quad (27)$$

where $Q_{\lambda,\text{abs}}^{\text{SiC}}(a_{\text{cl}})$ is the absorption efficiency factor of SiC grain with radius a_{cl} whose value is set to be $10^{-3} \mu\text{m}$ in the calculation, and $n_{\text{gas},j}$, m_j , and $C_{V,j}$ are the number density, the mass, and the specific heat at constant volume of the j -th gas species, respectively.

4.3. Modeling procedure

The models of pulsation-enhanced dust-driven wind are specified by the six parameters; the stellar mass M_* , the stellar luminosity L_* , the effective temperature T_{eff} , the C/O ratio, the period of the pulsation P , and the velocity amplitude of the pulsation Δu_p . As the first step of the hydrodynamical simulation, a dust-free static model atmosphere is constructed as follows; The initial stellar radius R_* is given by the Stefan-Boltzmann law $L_* = 4\pi R_*^2 \sigma T_{\text{eff}}^4$ where σ is the Stefan-Boltzmann constant. Given a guess value for gas density at R_* , the radial profiles of density and temperature are calculated by solving the equation

$$\frac{1}{\rho} \frac{dp}{dr} = -\frac{GM_*}{r^2} \quad (28)$$

coupled with the radiative transfer calculation with sufficiently fine grids. The procedure is iterated until the geometrically diluted optical depth at R_* converges to 2/3.

The dynamical model calculations including the formation of grains are carried out by placing the piston at $R_{\text{in}0}$ whose position is two times pressure scale height around R_* below from the photosphere of static model atmosphere and is defined as the inner boundary of dynamical model at $t=0$. Then the radius $R_{\text{in}}^{\text{dyna}}$ of inner boundary is varied sinusoidally with time as

$$R_{\text{in}}^{\text{dyna}} = R_{\text{in}0} + \Delta u_p \frac{P}{2\pi} \sin\left(\frac{2\pi}{P}t\right) \quad (29)$$

and the velocity $u_{\text{in}}^{\text{dyna}}$ at the inner boundary is given by

$$u_{\text{in}}^{\text{dyna}} = \Delta u_p \cos\left(\frac{2\pi}{P}t\right). \quad (30)$$

In the simulation, no mass flow is assumed through the inner boundary. The radiative flux is assumed to be constant over time and be equal to $\pi B(T_{\text{eff}}) = \pi \int_0^\infty B_\lambda(T_{\text{eff}})d\lambda$ at the photosphere of dynamical model R_{pht} where the diluted optical depth of gas is 2/3, and thus the stellar luminosity $L_* = 4\pi R_{\text{pht}}^2 \sigma T_{\text{eff}}^4$ varies with time. The piston velocity amplitude Δu_p is increased slowly from 1 cm s^{-1} to the specified value to prevent the first outwardly moving subsonic wave from growing into a enormous transient shock, following Bowen (1988).

After the onset of dust formation, the dust-driven wind takes places. As the gas expands, the spacing between radial grids in the acceleration region becomes wider and the rezoning procedure necessary for resolving the density structures of the circumstellar envelope is introduced by adopting the method proposed in Fleischer et al.(1992). After the outermost zone passes through the outer boundary of dynamical model which is placed at 25 R_* in the simulation, the outermost Lagrangian grid is eliminated. Then, at the outer boundary, we trace the time variations of mass-loss rate, gas outflowing velocity, dust-to-gas mass ratio, and condensation efficiency f_C (f_{Si}) which is defined as the fraction of carbon (silicon) atoms in C-bearing molecules except for CO (Si-bearing molecules) locked into carbon (SiC) grains. Note that, in the case that all Si atoms in Si-bearing molecules are locked into SiC grains, the maximum value of $f_C \sim 0.9$ in the model with C/O=1.4.

5. RESULTS

We adopt the following model parameters in the calculation; $T_{\text{eff}}=2600$ K, $L_*=10^4 L_\odot$, $M_*=1.0 M_\odot$, C/O=1.4, $P=650$ days, and $\Delta u_p=2.0$ km s^{-1} , which is a typical set of the values in the previous studies (e.g., Fleischer 1994; Winters et al. 2000) and is employed as the reference values in the models of C-rich AGB stars that reasonably reproduce the observed dynamical behaviors (Winters et al. 1994, 1997; Nowotny et al. 2005). The number of radial grids used in the hydrodynamical calculations depends on the density structure and is in the range between 800 and 1200 throughout the calculations. The wavelength region covered in the radiative transfer calculation

ranges from 0.35 to 120 μm and the number of wavelength grids is 100. The simulations have been performed for 180 cycles (stellar pulsation periods). In this paper, we neglect the radiation pressure force acting on SiC grains because of the transparency in the optical to infrared region (up to $\sim 9 \mu\text{m}$) (Choyke & Palik 1985; Pitman et al. 2008; Hofmeister et al. 2009).

The formation of SiC grains in the pulsation–enhanced dust–driven wind is closely related with the formation of carbon dust shell stemming from the rapid formation of carbon grains in the high density gas induced by the stellar pulsation and the resulting acceleration of dense region caused by the radiation pressure force acting on the carbon grains. The carbon dust shell is characterized by the inversions of density distributions of gas and carbon grains and plays a crucial role in the time evolution of gas temperature and density through the backwarming caused by the thermal emission from carbon grains. First, we outline the formation of carbon dust shells in this model, and then we show how SiC grains form in the LTE and non–LTE cases.

5.1. Formation of carbon dust shells

The carbon dust shell appears in the present model quasi–periodically once a stellar pulsation period and is classified into two types by the peak value of f_C in the shell. Here we shall overview the formation of each type of the carbon dust shells and its dynamics, referring Figure 2 which displays the radial structure of the quantities related to gas dynamics and formation of carbon and SiC grains in the LTE case throughout the period from $t=166.7$ to $168.8 P$.

The first type of carbon dust shell (hereafter referred to as the 1st type CDS) is defined as the high density region with the peak value of $f_C \gtrsim 0.9$, and is located around $4 R_*$ at $t=167.9 P$ (see the bottom row in Figure 2). The formation of this 1st type CDS actually starts at $t \sim 166.7 P$ and the behavior of formation process is almost the same as that of the 1st type CDS whose formation starts at $t \sim 168.8 P$; the nucleation of carbon grains takes place in the dust–free region ranging from 1.8 to $3.0 R_*$ whose gas temperature decreases to 1300 K (see the radial variation of the nucleation rate of carbon grains at $t=168.8 P$ and the time variation of the distribution of the number of carbon grains in this region from $t=168.5$ to $168.8 P$). Then, the backwarming by thermal emission from carbon grains subsequently formed in the outer part of this region not only raises up the gas temperature but also evaporates the carbon grains in the inner part (see the 3rd rows at $t=167.0 P$ and $t=167.3 P$). However, in the outer part, the nucleation and growth of carbon grains still proceed and the ratio of radiation pressure force to gravity α around $2.5 R_*$ exceeds unity at $t=167.0 P$ with increasing the volume equivalent radius $\langle a_C \rangle$ and the condensation efficiency f_C of carbon grains up to $\sim 0.1 \mu\text{m}$ and ~ 0.3 (see the 3rd and bottom rows), as a result this part is accelerated outwards. On the other hand, the gas density in the region outer than the accelerated region is insufficient to produce abundant enough carbon grains to accelerate this region efficiently despite the ongoing nucleation. Thus, the radial compression due to the velocity difference causes the outer part of the accelerated region to accelerate more through the increase of nucleation and growth rates of carbon grains, and results in the shell structure; note that the

shell structure is not associated with the pulsation shock but induced by the formation of carbon grains. The shell structure becomes prominent with decreasing the gas density in the region inner than the accelerated region due to the radial expansion (see the 2nd rows from $t=167.3$ to $167.6 P$). The formation of 1st type CDS completes at $t \sim 167.9 P$.

The formation of the second type of carbon dust shell (hereafter referred to as the 2nd type CDS) defined as the high density region with the peak value of $0.3 \lesssim f_C \lesssim 0.7$ onsets around $2.2 R_*$ at $t=168.2 P$, being triggered by the merging of the two consecutive shocks induced by the stellar pulsations, which can be seen from the time variations of gas velocity and α in this region from $t=167.9$ to $168.2 P$; the carbon grains in front of the precedent shock, which nucleated at $t \sim 166.7 P$ and survived from the evaporation process associated with the evolution of 1st type CDS starting at $t \sim 167.0 P$, grow up from $\langle a_C \rangle = 0.05$ to $0.1 \mu\text{m}$ in the region compressed further by the merging with the following shock (see the bottom rows from $t=167.6$ to $168.2 P$). After then, the nucleation and growth of carbon grains in the compressed outer part of this region develops the shell structure with increasing α , while the rapid decrease of gas density caused by the outward velocity already exceeding 10 km s^{-1} suppresses the growth rate of carbon grains and the increase of f_C . The evolution of this carbon dust shell ends up as the 2nd type CDS with the peak value of $f_C \sim 0.7$ at $t \sim 169.0 P$. The density profile as well as the peak value of f_C of 2nd type CDS varies from cycle to cycle (e.g., see the 2nd type CDS located around $4.5 R_*$ at $t=167.0 P$). The alternating formation of the 1st and 2nd type CDSs is sometimes disturbed, in which case the 2nd type CDS fails to grow up without increasing the peak value of f_C up to 0.3. The appearance and periodicity of carbon dust shell depend on the stellar parameters in a complicated manner as investigated by Fleischer et al. (1995), Höfner et al. (1995), and Dreyer et al. (2009, 2011). For example, in our model with $\text{C/O}=1.8$, only the 1st type CDS forms every stellar pulsation period.

5.2. Formation of SiC grains in LTE case

The values of mass-loss rate, gas terminal velocity, and dust-to-gas mass ratio averaged over the last sixty pulsation periods at the outer boundary are $1.24 \times 10^{-5} M_\odot \text{ yr}^{-1}$, 20.4 km s^{-1} , and 1.64×10^{-3} , respectively, in the hydrodynamical model with the LTE case for the formation of SiC grains. As can be seen from Figure 2, the nucleation of SiC grains onsets when the gas cools down to 1100 K after the formation of carbon grains, and is activated in the temperature range of 800–1000 K. The corresponding formation region is located around $3.5 \sim 5.5 R_*$ unless the gas temperature is raised up higher than 1100 K by the backwarming from the precedent 1st or 2nd type CDS. In the formation region, Si_2C_2 molecule is more abundant than SiC molecule and the nucleation proceeds through the reaction (2) rather than the reaction (1). In particular, the formation of SiC grains is most efficient in the region around the outer boundary of the 1st type CDS because of the lower temperature and higher gas density, and the nucleation rate per H-element reaches the maximum value of $\sim 10^{-25} \text{ s}^{-1}$ at $t=167.9 P$. However the subsequent decrease of the gas density caused by the accelerated radial expansion depresses the nucleation and growth processes of SiC

grains; the number of SiC grains per H–element is limited to smaller than 10^{-17} (see the bottom row at $t=168.8 P$), and the volume equivalent radius of SiC grains $\langle a_{\text{SiC}} \rangle$ is typically $3\text{--}6 \times 10^{-2} \mu\text{m}$. In the other regions, the number and size of SiC grains are much smaller. Thus the depletion of Si–bearing molecules does not take place substantially in LTE case (see the radial variation of f_{Si} in the bottom row throughout the time), and almost all of SiC grains form around the outer boundary of carbon dust shell.

Figure 3 represents the the radial distribution of gas and grains in the region of $r < 25 R_*$ at $t=166.8 P$. The radial distribution of f_{C} (the 2nd row) clearly shows that the different type of carbon dust shell forms by turns as addressed in Section 5.1. The carbon dust shells broaden with moving outwards from the formation sites because the outer part with more abundant carbon grains is accelerated more efficiently than the inner part, and the broadening in the outer circumstellar envelope of $r > 10 R_*$ is caused by the pressure gradient. In addition, the slower moving 2nd type CDS seems to be caught up by the faster moving 1st type CDS around $21 R_*$. Note that the shell (shock) structure seen in the radial distribution of gas density precedes the corresponding carbon dust shell in the outer circumstellar envelope (see the top row). The distributions of ρ_{SiC} (the top row) and f_{Si} (the 2nd row) demonstrate that SiC grains reside in thin shell around the outer boundary of carbon dust shell, reflecting the formation site. The value of f_{Si} ($\rho_{\text{SiC}}/\rho_{\text{gas}}$) and the mass ratio of SiC to carbon grains SiC/C are at most 10^{-6} (10^{-9}) and 10^{-6} , respectively (see the lower three rows). The value of f_{C} ($\rho_{\text{C}}/\rho_{\text{gas}}$) averaged over the last sixty pulsation periods at the outer boundary is 0.707 (1.64×10^{-3}), while the averaged value of f_{Si} ($\rho_{\text{SiC}}/\rho_{\text{gas}}$) is in the order of magnitude of 10^{-8} (10^{-11}). The resulting averaged value of SiC/C is 4.93×10^{-8} which is much smaller than the value inferred from the radiative transfer models (0.01–0.3).

Figure 4 shows the size distribution of SiC grains by mass averaged over the last sixty pulsation periods at the outer boundary. The distribution is characterized by the single–peaked profile with the peak around $a=6.0 \times 10^{-2} \mu\text{m}$, and the radius of SiC grains is limited to be less than $0.1 \mu\text{m}$. The modal size is almost a factor of four smaller than the size of presolar SiC grains extracted from the Murchison meteorite (Amari et al. 1994). The LTE case with lower C/O ratio resulting in lower gas outflow velocity makes the formation of SiC grains with radius of $0.2\text{--}0.3 \mu\text{m}$ possible as long as the gas outflow exhibits a layered structure with the CDSs. On the other hand, regardless of C/O ratio, the amount of SiC grains formed in the LTE case is too small to reproduce amount of SiC grains inferred from astronomical observations.

5.3. Formation of SiC grains in non–LTE case

Figure 5 displays the radial structure of the quantities related to gas dynamics and formation of grains in the non–LTE case throughout the period from $t=166.7$ to $168.8 P$. The vibration temperature of SiC cluster defined in Section 4.2 and depicted in the top row (solid red) is evaluated by placing the small SiC grain with $a_{\text{cl}}=10^{-3} \mu\text{m}$ hypothetically in the dynamical calculations. The difference between the gas temperature T_{gas} and the vibration temperature T_{v} is negligible in the

high density region of $\rho > 10^{-12}$ g cm $^{-3}$ where the collision with gas dominates the energy balance and controls T_v . As the gas density decreases and the collision with gas gets less effective than the interaction with the radiation in the energy balance, T_v deviates from and turns to be lower than T_{gas} because small SiC grain is almost transparent from the visible to infrared region (up to ~ 9 μm) (Choyke & Palik 1985; Pitman et al. 2008; Hofmeister et al. 2009). Also, it should be noted that T_v is not affected so much by the backwarming due to the thermal emission from the outer carbon dust shell compared with the gas temperature. Thus, the temperature difference $\Delta T = T_{\text{gas}} - T_v$ is magnified in the less dense region inner than the opaque carbon dust shell (e.g., see around $2.5 R_*$ at $t=167.3 P$).

As the gas density decreases, the supersaturation ratio of SiC grains quickly exceeds unity with increasing ΔT as well as decreasing T_v . The nucleation process of SiC grains can be activated in the region with $\rho < 10^{-12}$ g cm $^{-3}$ as long as $T_v \lesssim 1200$ K and $\Delta T \gtrsim 200$ K, even in the region with $T_{\text{gas}} \gtrsim 1400$ K where the nucleation process of carbon grains is almost depressed. On the other hand, if T_v is higher than 1200 K, the nucleation process of SiC grains is not activated regardless of the gas temperature since the abundances of molecules responsible for formation of SiC grains are not sufficient to make the supersaturation ratio large enough for the onset of nucleation.

The active nucleation and growth of SiC grains takes place in the infalling gas around $1.8\text{--}2.2 R_*$ at $t=166.7 P$ when the gas density drops down to a few times 10^{-13} g cm $^{-3}$, T_v decreases down below 1200 K and ΔT increases by larger than ~ 200 K, almost concurrently with the onset of formation of the 1st type CDS as explained in Section 5.1. Then, the backwarming from the evolving 1st type CDS raises up T_v and T_{gas} high enough so as to evaporate SiC grains in the inner dense region with $\rho \gtrsim 10^{-13}$ g cm $^{-3}$ at $t=167.0 P$. However, in the outer less dense region, SiC grains grow up to ~ 0.3 μm thanks to the increase of ΔT and the condensation efficiency f_{Si} reaches 0.1. In the region around $2.5 R_*$, the nucleation of SiC grains proceeds, and at $t=167.3 P$ the increase of f_{Si} is distinguishable while carbon grains evaporate due to the backwarming, which continues up to $t \sim 167.5 P$ (see the 3rd and bottom rows). On the other hand, in the region around $2 R_*$, the evaporation of SiC grains turns to the growth at $t=167.3 P$ with weakening the backwarming as the 1st CDS moves outwards, and then the increase of gas density up to 10^{-13} g cm $^{-3}$ caused by the pulsation shock leads to the efficient nucleation and growth of SiC grains, and f_{Si} increases up to ~ 0.7 quickly until $t=167.6 P$. Then, the efficient growth of SiC grains in the region compressed by the merging of consecutive shocks starting from $t \sim 167.9 P$ results in the complete consumption of Si-bearing molecules ($f_{\text{Si}}=1.0$) around $t \sim 168.1 P$, and $\langle a_{\text{SiC}} \rangle$ in this region is typically larger than ~ 0.2 μm , in contrast to the LTE-case. The region with the condensation efficiency $f_{\text{Si}} \sim 1.0$ is referred to as the Si-depletion region hereafter. Concurrently, the 2nd type CDS formed and developed in this region stretches the Si-depletion region outwardly (see the radial distribution of f_{Si} in the bottom row from $t=168.2$ to $168.8 P$), while the backwarming from the 2nd type CDS makes T_v higher than 1200 K and depresses the nucleation of SiC grains in the region inner than the Si-depletion region for a while (see T_v in the top row at $t=168.5 P$). It should be noted that the 2nd type CDS moves outward more slowly than the 1st type CDS as mentioned in Section 5.2.

Thus, the Si–depletion region with slower outward velocity is finally caught up and pushed by the 1st type CDS as can be seen from the time evolution of the Si–depletion region spreading over from 3.5 to 5.5 R_* at $t=167.3 P$ which formed two cycles before.

As mentioned above, the formation of Si–depletion region onsets in the infalling gas in front of the coming pulsation shock, and the region moves outward with the formation of 2nd type CDS triggered by the merger with the next pulsation shock. Thus, the Si–depletion region forms once every two pulsation periods. Also, even in the other regions, the resulting value of f_{Si} often exceeds 0.1. Thus, in contrast to the very small value of at most 10^{-6} in LTE case, a large amount of SiC grains can condense through the inverse greenhouse effect in the non–LTE case.

Figure 6 presents the radial variations of gas and grains at $t=176.3 P$. It seems that SiC grains are concentrated around the outer boundaries of 1st type CDSs in the density distribution (see the top row) because the shock associated with the formation of carbon dust shell sweeps up the gas. Reflecting the variation of gas density, the radial distribution of ρ_{SiC} does not always corresponds to the Si–depletion region shown in the 2nd row. It should be noted that the extended Si–depletion region does not develop without the 2nd type CDS, which can be demonstrated from an example of the failure of alternating formation of both types of carbon dust shells located at 18 R_* where Si–depletion region restricted in a narrow region resides just ahead of the 1st type CDS formed about 1 cycle after from the formation of the Si–depletion region (see the 2nd row). Apart from the 1st type CDS located at 18 R_* , the extended SiC dust shell corresponding to the Si–depletion region between 1st and 2nd type CDSs can be clearly recognized in the radial distribution of $\rho_{\text{SiC}}/\rho_{\text{gas}}$ (see the 3rd row where $\rho_{\text{SiC}}/\rho_{\text{gas}}=8.46\times 10^{-4}$ corresponding to $f_{\text{Si}} = 1.0$). The radial distribution of f_{Si} shows that the Si–depletion region stretched over by the slower moving 2nd type CDS narrows with moving outwardly, being compressed by the faster moving 1st type CDS. Thus, in the outer circumstellar envelope, the radial width tends to be of the order of the stellar radius (see f_{Si} around 24 R_* where the 2nd type CDS almost merges with the 1st type CDS) and the narrower Si–depletion region seems to reside around the outer boundary of the 1st type CDS.

The radial distribution of the mass ratio SiC/C has a sharp peak in the region just ahead of the outer boundary of 1st type CDS, and decrease by 0.1 (10^{-4}) toward the outer boundary of precedent 2nd (1st) type CDS (see the bottom row). The peak value exceeds ten in the inner circumstellar envelope, and decreases with increasing r because of the subsequent growth of carbon grains. However the value of SiC/C in the Si–depletion region still keeps larger than 0.2 with the peak value exceeding unity.

The resulting values of mass–loss rate, terminal velocity, dust–to–gas mass ratio averaged over the last sixty stellar pulsation periods are $1.10\times 10^{-5} M_{\odot} \text{ yr}^{-1}$, 19.5 km s^{-1} , and 1.85×10^{-3} , respectively, for the non–LTE case. The reduction of terminal velocity compared to the LTE case reflects the somewhat weakened acceleration resulting from the reduction of amount of carbon grains due to the incorporation of C–bearing gas species into SiC grains; on average 4.40 % of carbon atoms in the condensible C–bearing molecules is incorporated into the SiC grains. The averaged

value of ρ_C/ρ_{gas} (f_C) is 1.51×10^{-3} (0.652), while the value of $\rho_{\text{SiC}}/\rho_{\text{gas}}$ (f_{Si}) is 3.41×10^{-4} (0.403). The resulting averaged value of SiC/C is 0.226 and is close to the upper value derived from the radiative transfer models. The size distribution of SiC grains by mass averaged over the last sixty stellar pulsation periods at the outer boundary is depicted in Figure 7. The size distribution shows the broad profile with the mean radius of $0.3 \mu\text{m}$, in contrast to the sharp and single-peaked size distribution in the LTE case presented in Figure 4. In the size range from 0.03 to $4.0 \mu\text{m}$, 80 % of SiC grains by mass populate in the radii between 0.2 and $1.0 \mu\text{m}$: The distribution well covers the size range of presolar SiC grains found in the Murchison meteorite. Thus the hydrodynamical model with the non-LTE case for the formation of SiC grains that the vibration temperature of SiC cluster is assumed to be the same as the temperature of small SiC grains reasonably reproduces the amount of SiC grains inferred from astronomical observations and the size of presolar SiC grains extracted from the Murchison meteorite.

6. DISCUSSION

In the calculations of hydrodynamical models presented in Section 5, we assume that SiC is the starting molecule for the nucleation process of SiC grains, excluding the process starting from the two-body reaction of Si_2C_2 molecules. This may underestimate the amount of SiC grains in the LTE case since Si_2C_2 molecule is more abundant in the lower temperature region than SiC molecule as shown in Figure 1 (left). In the LTE case where carbon grains condense in prior to SiC grains, the nucleation process starting from the two-body reaction of Si_2C_2 molecules dominates the nucleation rate in the region around $6\text{--}8 R_*$ whose gas temperature ranges from 600 to 800 K. However the gas density in the region of $\rho \sim 10^{-16} \text{ g cm}^{-3}$ is too low to increase the amount of SiC grains; even if this process is included in the calculation, the resulting values of both f_{Si} and SiC/C are limited to 10^{-4} although the nucleation rate is much larger than that starting from SiC molecule. In addition, this nucleation process produces the population of grains whose radii are much smaller than $6.0 \times 10^{-2} \mu\text{m}$, and make the modal radius smaller than $3.0 \times 10^{-2} \mu\text{m}$. Thus the nucleation process starting from two-body reaction of Si_2C_2 molecules does not change the conclusion that the hydrodynamical models with the LTE-case cannot reproduce the amount of SiC grains around C-rich AGB stars inferred from the astronomical observation and the size range derived from the analysis of presolar grains.

In the non-LTE case, this nucleation process dominates the formation of SiC grains in the region of $r > 4 R_*$, and is activated particularly in the outer part of the carbon dust shell. Although the number of SiC grains produced through this process reaches about 10 times that produced through the nucleation starting from SiC molecule, the typical radius of SiC grains formed in the region with low gas density is limited to $3 \times 10^{-3}\text{--}6 \times 10^{-2} \mu\text{m}$. Thus, the inclusion of this nucleation process does not affect the size distribution of SiC grains whose radius is larger than $0.1 \mu\text{m}$. Also it is true for the amount of SiC grains since the averaged f_{Si} increases by only a few percent. Thus we conclude that the exclusion of nucleation process starting from the two-body reaction of

Si₂C₂ molecules does not affect the result of calculations in the non-LTE case, except for the size distribution in the range of $a_{\text{SiC}} < 6 \times 10^{-2} \mu\text{m}$.

The sticking probability set to be unity for nucleation and growth processes of SiC grains may overestimate the size and amount of SiC grains formed in the non-LTE case. Figure 8 shows the time averaged size distributions by mass of SiC grains for given values of α_s . In the range of $\alpha_s=0.1-1.0$, the mass fraction of large sized grains with $a > 1.0 \mu\text{m}$ decreases significantly and the profile becomes narrow with decreasing α_s , while the reduction of α_s does not affect the mass fraction of small-sized grains with $a \leq 0.1 \mu\text{m}$. The modal radii are 0.30 and 0.22 μm for $\alpha_s=0.5$ and 0.1, respectively. Although the SiC grains with radii larger than 1.0 μm do not form for the case of $\alpha_s=0.1$, the hydrodynamical models in the non-LTE case reasonably reproduce the size range of presolar SiC grains extracted from the Murchison meteorite (Amari et al. 1994) as long as $\alpha_s \gtrsim 0.1$. The averaged value of SiC/C decreases with decreasing α_s ; the values are 0.199 and 9.77×10^{-2} for $\alpha_s=0.5$ and 0.1, respectively, which is within the range of the value inferred from the radiative transfer models. Although the reduction of α_s changes the radial distribution of SiC grains substantially, we conclude that the hydrodynamical models in the non-LTE case cover the ranges of size derived from the analysis of presolar grains and amount evaluated from the radiative transfer models unless the sticking probability $\alpha_s \lesssim 0.1$.

The mass ratio of SiC/C inferred from the radiative transfer models depends on the models used in the calculation; the evaluated values for C-rich AGB stars with the emission feature of SiC grains are in the range of 0.01–0.29 (Lorenz-Martins & Lefèvre 1994), 0.01–0.15 (Groenewegen 1995; Groenewegen et al. 1998), and 0.1–0.3 (Blanco et al. 1998). The smaller value by Groenewegen (1995) and Groenewegen et al. (1998) is considered to be ascribed to the grain model; the temperature of composite grain consisting of carbon and SiC used in their model is higher than that of isolated SiC grains used in the other models as is shown in Blanco et al. (1998), since carbon grains are more absorptive in the visible to NIR region than SiC grains. Therefore, in order to reproduce the observed SEDs, if the inner boundary of dust layer is placed close to the photosphere, the high temperature of composite grains causes the value of SiC/C to reduce. Also, the smaller value of 0.01–0.06 derived by Lorenz-Martins & Lefèvre (1994) for C-rich AGB stars showing SiC emission feature with optically thick shells ($\tau_{1\mu\text{m}} > 3.0$) would arise from the optical constant of SiC grains used in the models; the radiative transfer models usually employ the optical constants derived from the SiC powder synthesized in the laboratory (Borghesi et al. 1985; Pégourié 1988). The absorption coefficients in visible to infrared region (up to $\sim 9 \mu\text{m}$) is much larger than the crystalline SiC (Choyke & Palik 1985; Pitman et al. 2008; Hofmeister et al. 2009), which results in the higher temperature of SiC grains and the smaller SiC/C. In addition, the mid-infrared observation of C-rich AGB stars by *Spitzer* shows that the 30 μm emission feature attributed to MgS grains becomes prominent with decreasing the strength of SiC emission feature in the stars with mass-loss rate larger than $10^{-6} M_{\odot} \text{yr}^{-1}$ (Leisenring et al. 2008). Zhukovska & Gail (2008) demonstrates that the absorption efficiency around 11.3 μm of grains consisting of a SiC core and a MgS mantle decreases with increasing the volume fraction of MgS mantle. Therefore, if it is true,

the radiative transfer model could underestimate the value of SiC/C without including SiC grains coated by MgS mantle. Thus, the mass ratio of SiC to carbon grains derived from the radiative transfer models depends on the optical constants of SiC as well as the model of grains used in the calculations, and the value of SiC/C up to ~ 0.23 calculated in the non-LTE case for C-rich AGB stars is considered to be not always in conflict with the values derived from SED fittings.

7. SUMMARY

The formation of SiC grains around C-rich AGB stars is investigated for the first time in the framework of hydrodynamical model for the pulsation-enhanced dust-driven wind. We formulate the nucleation and growth processes of SiC grains, considering that SiC grains nucleate and grow homogeneously starting from SiC molecule. In the calculations, the two cases are considered for the nucleation process of SiC grains; the LTE case in which the vibration temperature T_v of SiC cluster is equal to the gas temperature and the non-LTE case in which T_v is assumed to be the same as the temperature of small SiC grain whose radius is $10^{-3} \mu\text{m}$. On the other hand, the vibration temperature of carbon cluster is considered to be the same as the gas temperature as is usually assumed in the hydrodynamical models for C-rich AGB stars.

The results of calculations for the model parameters $M_*=1.0 M_\odot$, $L_*=10^4 L_\odot$, $T_{\text{eff}}=2600 \text{ K}$, C/O ratio=1.4, $P=650 \text{ days}$, and $\Delta u_p=2.0 \text{ km s}^{-1}$ are summarized as follows: In the LTE case, SiC grains form in the accelerated and low-density outflowing gas after the formation of carbon grains. The resulting time averaged number fraction of Si atoms locked into SiC grains (condensation efficiency f_{Si}) of at most 10^{-8} is too small to reproduce the amount of SiC grains inferred from the astronomical observations and the radius is limited to less than $0.1 \mu\text{m}$. On the other hand, in the non-LTE case, the time averaged mass ratio of SiC to carbon grains ranges from 0.098 to 0.23 for the sticking probability $\alpha_s=0.1-1.0$, which is not in conflict with the value of 0.01–0.3 inferred from the radiative transfer models. The time averaged size distribution of SiC grains by mass with the peak at radius of $0.2-0.3 \mu\text{m}$ well covers the size range of presolar SiC grains extracted from the Murchison meteorite. Thus we conclude that the so called inverse greenhouse effect plays a crucial role in the formation process of SiC grains in the pulsation-enhanced dust-driven winds from C-rich AGB stars, apart from the validity of the underlying assumption made in the non-LTE case. The non-LTE effect should be explored for the formation process of dust grains in astrophysical environments.

The hydrodynamical model provides the two types of carbon dust shells; the 1st (2nd) type CDS with the peak value of $f_C \gtrsim 0.9$ ($0.3 \lesssim f_C \lesssim 0.7$). The formation region and the resulting radial distribution of SiC grains in the hydrodynamical model with non-LTE case is closely related with the formation and dynamics of carbon dust shell, especially through the density enhancement and the backwarming effect. In the inner circumstellar envelope, the SiC dust shell can be discriminated from the 1st type CDS through the extended Si-depletion region caused by the 2nd CDS formed in the outer part of active SiC formation region. However, in the outer circumstellar envelope of

$r > 20 R_*$, the SiC dust shell is localized around the outer boundary of 1st type CDS. Not only the formation region and the radial distribution but also the amount and the size distribution of SiC grains could heavily depend on the C/O ratio as well as the other model parameters; for instance, in the non-LTE case with $M_*=2.0 M_\odot$, the mass ratio of SiC to gas and the size of SiC are almost the same as those with $M_*=1.0 M_\odot$ while the mass loss rate decreases by a factor 5. Anyway more comprehensive study covering a wide range of model parameters is necessary for revealing the amount and the size distribution of SiC grains formed around C-rich AGB stars. Also, the difference between the radial distributions of carbon and SiC grains could greatly influence the appearance of the spectral feature attributed to SiC grains. These aspects will be investigated in the forthcoming papers.

We are grateful to the anonymous referee for valuable comments that improved the manuscript. We thank Dr. K. Ohnaka for his critical reading of the first draft and useful comments. This research has been partly supported by the Grant-in-Aid for Scientific Research of the Japan Society for the Promotion of Science (18104003, 20340038).

REFERENCES

- Allen, C. W. 1973, *Astrophysical Quantities*, The Athlone Press, London
- Allen, B. C., & Kingery, W. D. 1959, *Trans. Metal. Soc. AIME*, 215, 30
- Amari, S., Lewis, R. S., & Anders, E. 1994, *Geochim. Cosmochim. Acta*, 58, 459
- Bergeat, J., Knapik, A., & Rutily, B. 2002, *A&A*, 390, 987
- Bergeat, J., & Chevallerier, L. 2005, *A&A*, 429, 235
- Berman, R. G., & Brown, T. H. 1985, *Contr. Miner. Petrol.*, 89, 168
- Bernatowicz, T. J., Cowsik, R., Gibbons, P. C., et al. 1996, *ApJ*, 472, 760
- Bernatowicz, T. J., Fraundorf, G., Ming, T., et al. 1987, *Nature*, 330, 728
- Blanco, A., Borghesi, A., Fonti, S., & Orofino, V. 1994, *A&A*, 283, 561
- Blanco, A., Borghesi, A., Fonti, S., & Orofino, V. 1998, *A&A*, 330, 505
- Borghesi, A., Bussoletti, E., Colangeli, L., & de Blasi, C. 1985, *A&A*, 153, 1
- Bowen, G. H. 1988, *ApJ*, 329, 299
- Chase, M. W., Jr., Davies, C. A., Downey, J. R., Jr., et al. 1985, *J. Phys. Chem. Ref. Data*, 14, Suppl. 1

- Cherchneff, I., Barker, J.R., & Tielens, A.G.G.M. 1992, *ApJ*, 401, 269
- Choyke, W. J., & Palik, E. D. 1985, in *Handbook of Optical Constants of Solids*, Palik E.D. (ed.), Academic Press, Boston, p587
- Croat T. K., Stadermann, F. J., & Bernatowicz, T. J. 2005, *ApJ*, 631, 976
- Croat T. K., Stadermann, F. J., & Bernatowicz, T. J. 2010, *AJ*, 139, 2159
- Danchi, W. C., Bester, M., Degiacomi, C. G., McCullough, P. R., & Townes, C. H. 1990 *ApJ*, 359, L59
- Daulton, T. L., Bernatowicz, T. J., Lewis, R. S., et al. 2003, *Geochim. Cosmochim. Acta*, 67, 4743
- Deng, J. L., Su, K. H., Wang, X., et al. 2008, *Eur. Phys. J. D*, 49, 21
- Draine, B. T. 1985, *ApJS*, 57, 587
- Dreyer, C., Hegmann, M., & Sedlmayr, E. 2009, *A&A*, 499, 765
- Dreyer, C., Hegmann, M., & Sedlmayr, E. 2011, *A&A*, 525, A135
- Ferrarotti, A. S., & Gail, H.-P. 2006, *A&A*, 447, 553
- Fleischer, A. J. 1994, PhD thesis, Technische Universität, Berlin, FRG
- Fleischer, A. J., Gauger, A., & Sedlmayr, E. 1992, *A&A*, 266, 321
- Fleischer, A. J., Gauger, A., & Sedlmayr, E. 1995, *A&A*, 297, 543
- Gail, H.-P., & Sedlmayr, E. 1988, *A&A*, 206, 153
- Gauger, A., Gail, H.-P., & Sedlmayr, E. 1990, *A&A*, 235, 345
- Goebel, J. H., Bregman, J. D., Goorvitch, D., et al. 1980, *ApJ*, 235, 104
- Groenewegen, M. A. T. 1995, *A&A*, 293, 463
- Groenewegen, M. A. T., Whitelock, P. A., Smith, C. H., & Kerschbaum, F. 1998, *MNRAS*, 293, 18
- Hackwell, J. A. 1972, *A&A*, 21, 239
- Hasegawa, H., & Kozasa, T. 1988, *Prog. Theor. Phys. Suppl.*, 96, 107
- Helling, Ch., Winters, J. M., & Sedlmayr, E. 2000, *A&A*, 358, 651
- Hofmeister, A. M., Pitman, K. M., Goncharov, A. F., & Speck, A. K. 2009, *ApJ*, 696, 1502
- Höfner, S., Feuchtinger, M.U., & Dorfi, E.A. 1995, *A&A*, 297, 815

- Höfner, S., Fleischer, A. J., Gauger, A., et al. 1996, *A&A*, 314, 204
- Höfner, S. Gautschy-Loidl, R., Aringer, B., & Jørgensen, U., G. 2003, *A&A*, 399, 589
- Hoppe, P., Amari, S., Zinner, E., Ireland, T. & Lewis, R. S. 1994 *ApJ*, 430, 870
- Hoppe, P., & Ott, U. 1997, in *Astrophysical Implications of the Laboratory Study of Presolar Materials*, Bernatowicz, T. J. & Zinner, E. (ed.), AIP, New York, p27
- Hoppe, P., & Zinner, E. 2000, *J. Geophys. Res.*, 105, 10371
- Jones, B., Merrill, K. M., Puetter, R. C., & Willner, S. P. 1978, *AJ*, 83, 1437
- Kozasa, T., Dorschner, J., Henning, T., & Stognienko, R. 1996, *A&A*, 307, 551
- Kozasa, T., & Hasegawa, H. 1987, *Prog. Theor. Phys.*, 77, 1402
- Krüger, D., Woitke, P., & Sedlmayr, E. 1995, *A&AS*, 113, 593
- Leisenring, J. M., Kemper, F., & Sloan, G.C. 2008, *ApJ*, 681, 1557
- Lide, D. R. 2003, *CRC Handbook of Chemistry and Physics*, 84th ed., CRC Press, New York
- Lodders, K., & Fegley, B., Jr 1995, *Meteoritics*, 30, 661
- Lorenz-Martins, S., & Lefèvre, J. 1993, *A&A*, 280, 567
- Lorenz-Martins, S., & Lefèvre, J. 1994, *A&A*, 291, 831
- Mattsson, L., Wahlin, R., & Höfner, S. 2009, *A&A*, 509, A14
- McCabe, E., M. 1982, *MNRAS*, 200, 71
- Nowotny, W., Lebzelter, T., Hron, J., & Höfner, S. 2005, *A&A*, 437, 285
- Ott, U. in *Lecture Notes in Physics 815*, Henning, T. (ed.), Springer, Berlin, p277
- Pégourié, B. 1988, *A&A*, 194, 335
- Pitman, K. M., Hofmeister, A. M., Corman, A. B., & Speck, A. K. 2009, *A&A*, 483, 661
- Richtmyer R. D., & Morton, K. W. 1967, *Difference methods for initial value problems*, 2nd ed., John Wiley & Sons, New York
- Rouleau, F. & Martin, P. G. 1991, *ApJ*, 377, 526
- Russell, S. S., Ott, U., Alexander, C. M. O'd., Zinner, E., Arden, J. W., & Pillinger, C. T. 1997, *Meteorite. Planet. Sci.*, 32, 719
- Sharp, C. M., & Wasserburg, G. J. 1995, *Geochim. Cosmochim. Acta*, 59, 1633

- Speck, A. K., Barlow, M. J., & Skinner, C. J. 1997, MNRAS, 288, 431
- Speck, A. K., Corman, A. B., Wakeman, K., Wheeler, C. H., & Thompson, G. 2009, ApJ, 691, 1202
- Spitzer, W. G., Kleinman, D., & Walsh, D. 1959, Phys. Rev., 113, 127
- Stroud, R. M. & Bernatowicz, T. J. 2005, Lunar Planet. Sci., 36, 2010
- Treffers, R., & Cohen, M. 1974, ApJ, 188, 545
- Winters, J. M., Dominik, C., & Sedlmayr, E. 1994, A&A, 288, 255
- Winters, J. M., Fleischer, A. J., Le Bertre, T., & Sedlmayr, E. 1997, A&A, 326, 305
- Winters, J. M., Le Bertre, T., Jeong, K. S., Helling, Ch., & Sedlmayr, E. 2000, A&A, 361 , 641
- Woitke, P. 2006, A&A, 460, L9
- Woitke, P., & Niccolini, E. 2005, A&A, 433, 1101
- Yamasawa, D., Habe, A., Kozasa, T., et al. 2011, ApJ, 735, 44
- Zhukovska, S., Gail, H.-P., & Tieloff, M. 2008, A&A, 479, 453
- Zhukovska, S., & Gail, H.-P. 2008, A&A, 486, 229
- Zinner, E., Tang, M., & Anders, E. 1987, Nature, 330, 730

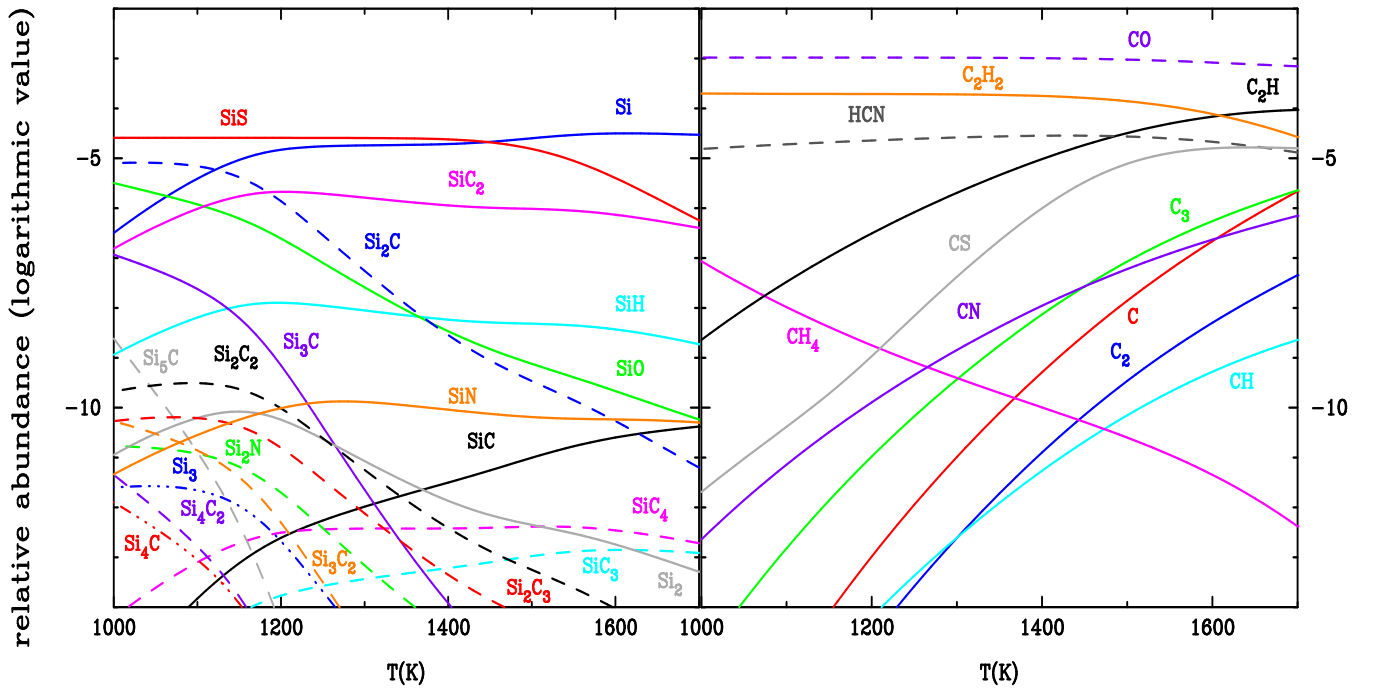


Fig. 1.— Relative abundances of Si-bearing molecules (left) and C-bearing molecules (right) in chemical equilibrium in the gas with the density $\rho = 10^{-13} \text{ g cm}^{-3}$ and C/O ratio = 1.4.

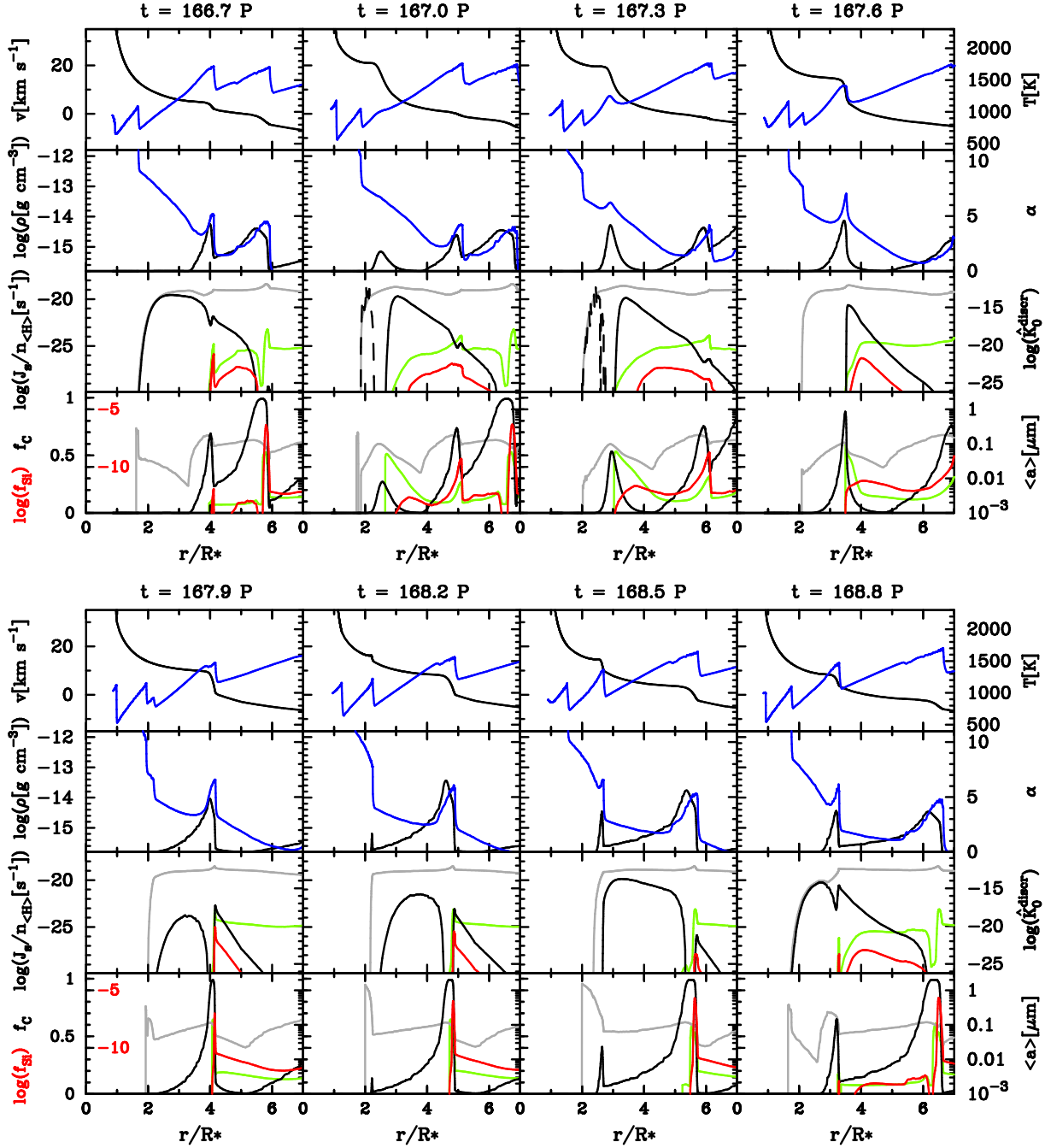


Fig. 2.— Radial structure in LTE case for $t=166.7$ to $167.6 P$ (top panel) and for $t=167.9$ to $168.8 P$ (bottom panel). Top row; the gas velocity v (blue) and the gas temperature T_{gas} (black). 2nd row; the gas density ρ (blue) and the ratio of radiation pressure force to gravity α (black). 3rd row; the nucleation rates per H–element $J_S/n_{\langle H \rangle}$ of carbon (black solid) and SiC (red) grains, the destruction rate per H–element $J_{\text{des}}/n_{\langle H \rangle}$ of carbon grains (black dashed), and the numbers per H–element \hat{K}_0^{discr} of carbon (grey) and SiC (green) grains. Bottom row; the condensation efficiencies f_C (black) and f_{Si} (red), and the volume equivalent radii $\langle a \rangle$ of carbon (grey) and SiC (green) grains.

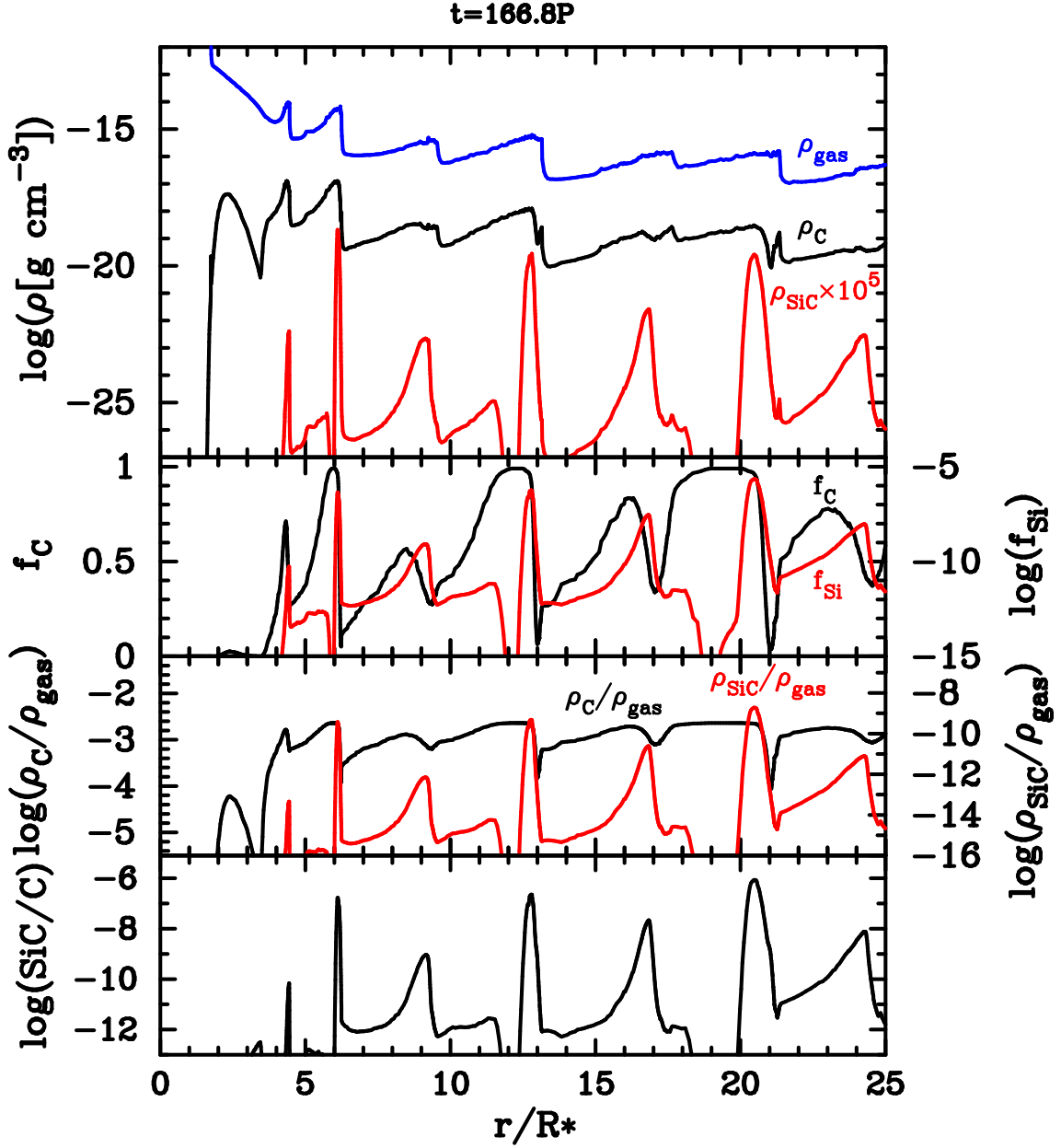


Fig. 3.— Radial distributions of gas and grains at $t=166.8 P$ in the LTE case. Top row; the mass densities of gas (blue, ρ_{gas}), carbon (black, ρ_{C}) and SiC (red, ρ_{SiC}) grains. 2nd row; the condensation efficiencies f_{C} (black) and f_{Si} (red). 3rd row; the density ratios of $\rho_{\text{C}}/\rho_{\text{gas}}$ (black) and $\rho_{\text{SiC}}/\rho_{\text{gas}}$ (red). Bottom row; the mass ratio of SiC to carbon grains SiC/C .

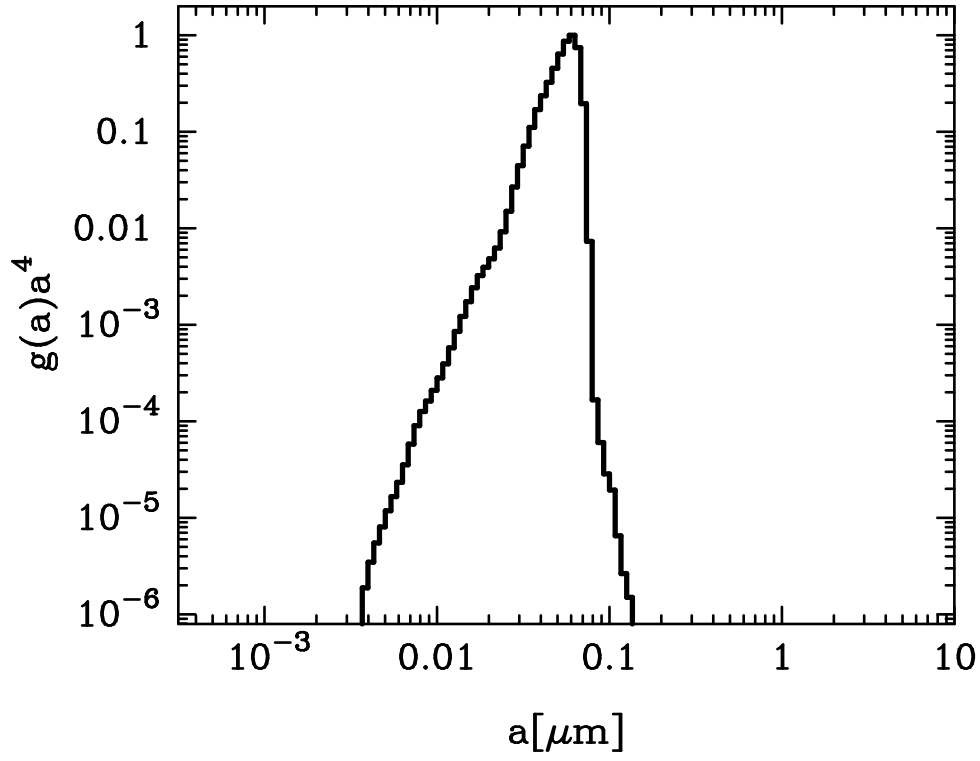


Fig. 4.— Size distributions of SiC grains by mass averaged over the last sixty stellar pulsations at the outer boundary in the LTE case. Note that $g(a)$ is the size distribution function and the value of $g(a)a^4$ is normalized to the maximum value.

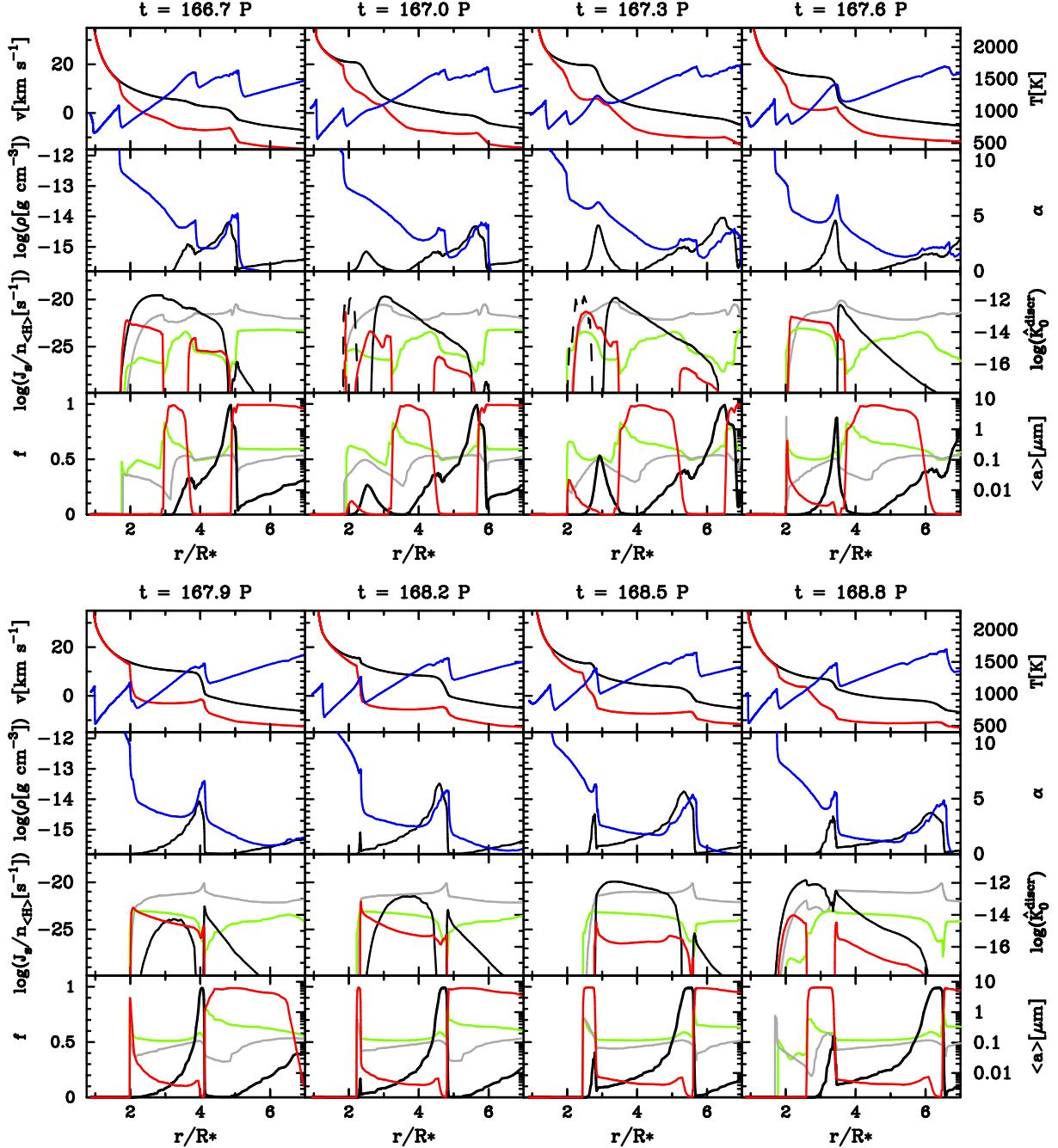


Fig. 5.— Same as Figure 2, but for the non-LTE case. Note that the red line in the top rows denotes the vibration temperature T_v and the red-dashed line around $1.9 R_*$ in the 3rd row at $t=167.0 P$ depicts the destruction rate of SiC grains per H-element $J_{\text{des}}/n_{\langle H \rangle}$.

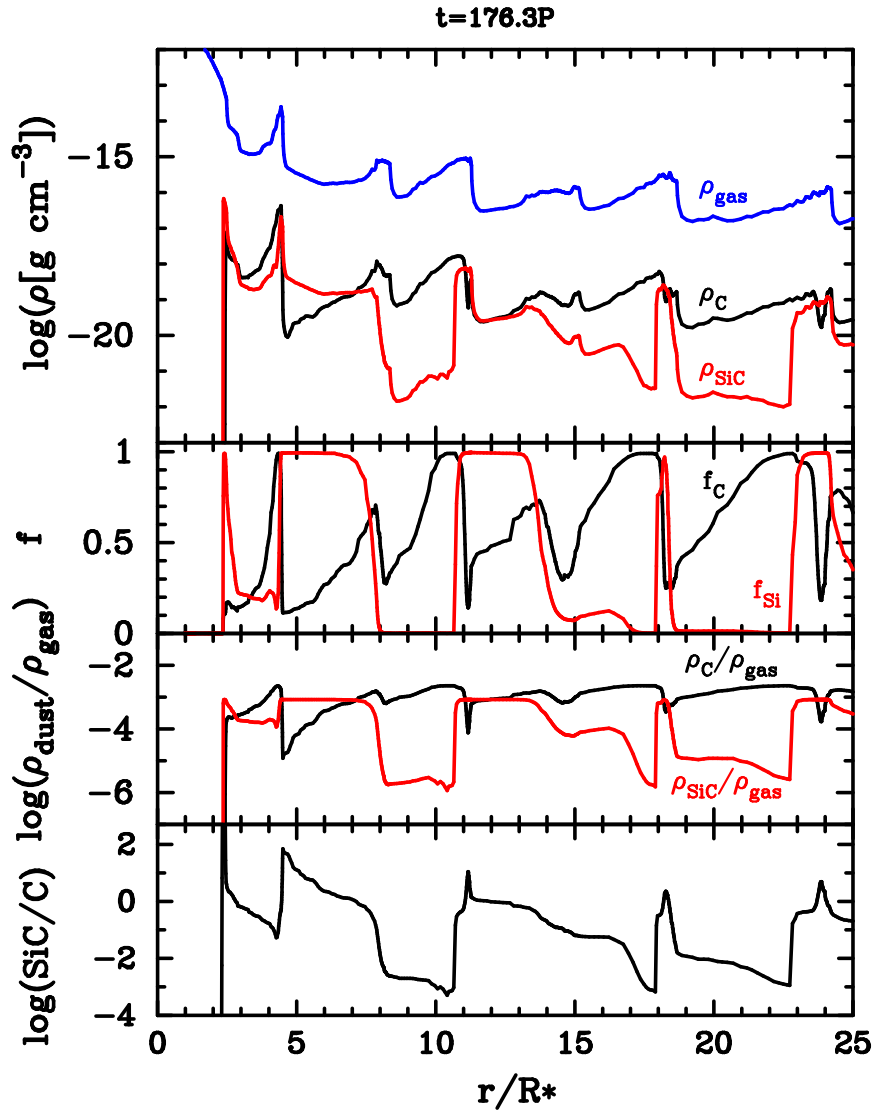


Fig. 6.— Same as Figure 3 but for $t=176.3P$ in the non-LTE case.

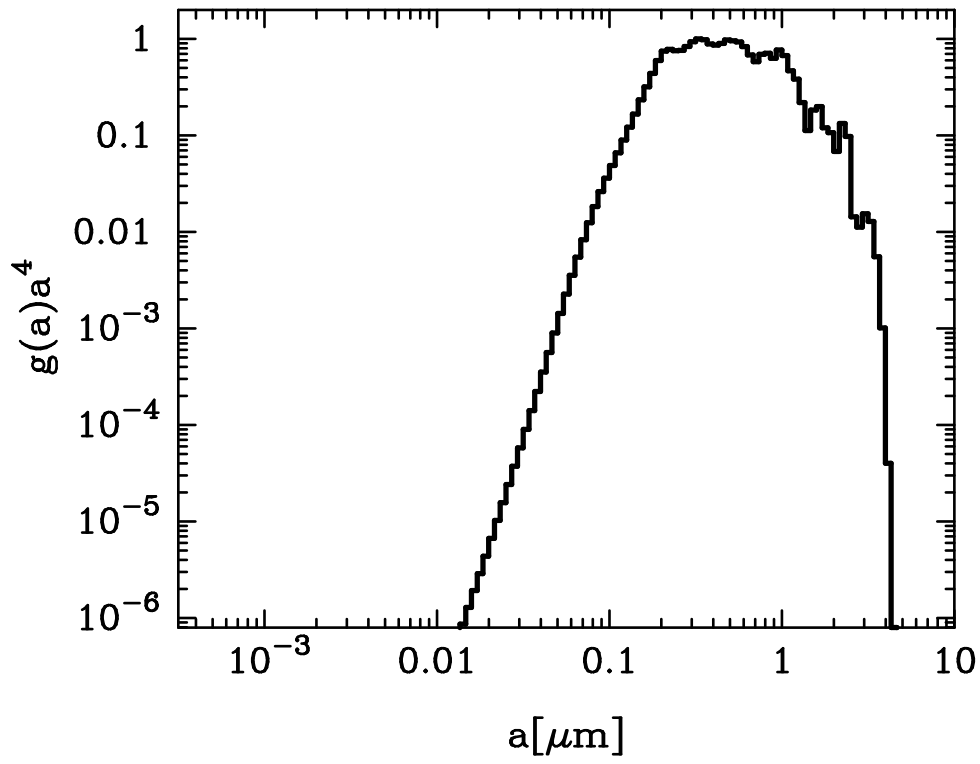


Fig. 7.— Same as Figure 4, but for the non-LTE case.

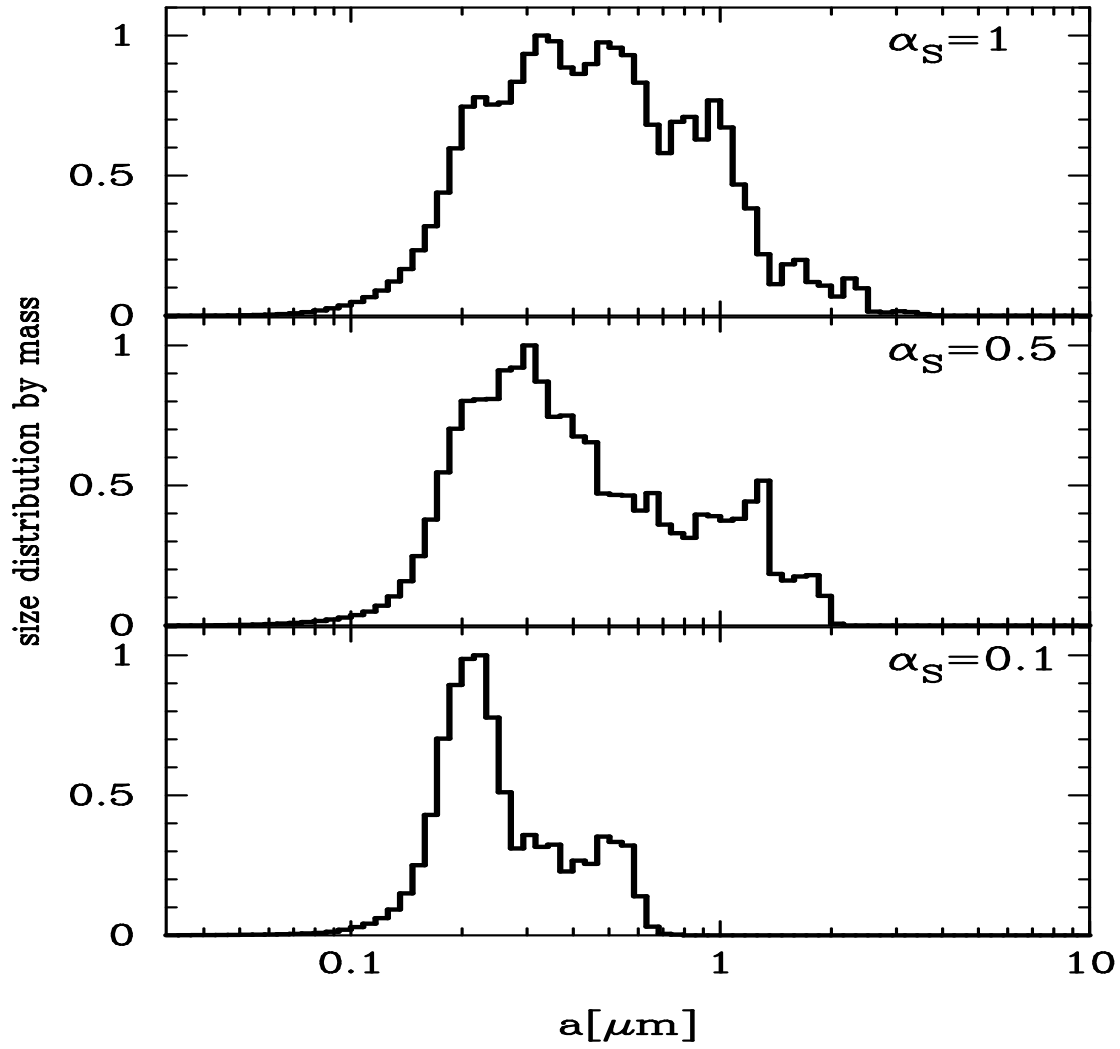


Fig. 8.— Averaged size distributions of SiC grains by mass for given values of α_S , each of which is normalized by the maximum value.

Table 1: Reaction enthalpies ΔH° for growth reactions of SiC cluster with size $n=2$ to 3.

Reaction	ΔH° [kJ mol ⁻¹]	
	1000K	1500K
SiC + SiC \rightarrow Si ₂ C ₂	-751.5	-751.0
SiC + Si ₂ C ₂ \rightarrow Si ₃ C ₃	-518.8	-514.5
SiC ₂ + SiC \rightarrow Si ₂ C ₂ + C	76.98	78.12
SiC ₂ + Si ₂ C ₂ \rightarrow Si ₃ C ₃ + C	309.6	314.7
SiC ₃ + SiC \rightarrow Si ₂ C ₂ + C ₂	-54.88	-58.76
SiC ₃ + Si ₂ C ₂ \rightarrow Si ₃ C ₃ + C ₂	177.8	177.8
SiC ₄ + SiC \rightarrow Si ₂ C ₂ + C ₃	-123.0	-131.1
SiC ₄ + Si ₂ C ₂ \rightarrow Si ₃ C ₃ + C ₃	109.7	105.4
Si ₂ C + SiC \rightarrow Si ₂ C ₂ + Si	-110.8	-109.8
Si ₂ C + Si ₂ C ₂ \rightarrow Si ₃ C ₃ + Si	121.9	126.7
Si ₂ C ₂ + Si ₂ C ₂ \rightarrow Si ₃ C ₃ + SiC	232.7	236.5
Si ₂ C ₃ + SiC \rightarrow Si ₂ C ₂ + SiC ₂	-199.5	-202.6
Si ₂ C ₃ + SiC \rightarrow Si ₃ C ₃ + C	110.1	112.1
Si ₂ C ₃ + Si ₂ C ₂ \rightarrow Si ₃ C ₃ + SiC ₂	33.14	33.97
Si ₃ C + SiC \rightarrow Si ₂ C ₂ + Si ₂	-53.73	-52.46
Si ₃ C + Si ₂ C ₂ \rightarrow Si ₃ C ₃ + Si ₂	178.9	184.1
Si ₃ C ₂ + SiC \rightarrow Si ₃ C ₃ + Si	-122.4	-119.9
Si ₄ C + SiC \rightarrow Si ₂ C ₂ + Si ₃	-122.6	-124.9
Si ₄ C + Si ₂ C ₂ \rightarrow Si ₃ C ₃ + Si ₃	110.1	111.6
Si ₄ C ₂ + SiC \rightarrow Si ₂ C ₂ + Si ₃ C	-195.5	-199.5
Si ₄ C ₂ + SiC \rightarrow Si ₃ C ₃ + Si ₂	-16.53	-15.41
Si ₄ C ₂ + Si ₂ C ₂ \rightarrow Si ₃ C ₃ + Si ₃ C	37.19	37.04
Si ₅ C + SiC \rightarrow Si ₂ C ₂ + Si + Si ₃	352.2	347.9
Si ₅ C + Si ₂ C ₂ \rightarrow Si ₃ C ₃ + Si + Si ₃	584.8	584.5

Table 2: Reaction enthalpies ΔH° for growth reactions of solid SiC.

Reaction	ΔH° [kJ mol ⁻¹]	
	1000K	1500K
SiC + SiC(s) \rightarrow 2SiC(s)	-793.8	-788.5
SiC ₂ + SiC(s) \rightarrow 2SiC(s) + C	34.64	40.66
SiC ₃ + SiC(s) \rightarrow 2SiC(s) + C ₂	-97.22	-96.22
SiC ₄ + SiC(s) \rightarrow 2SiC(s) + C ₃	-165.3	-168.6
Si ₂ C + SiC(s) \rightarrow 2SiC(s) + Si	-153.1	-147.3
Si ₂ C ₂ + SiC(s) \rightarrow 3SiC(s)	-836.2	-826.0
Si ₂ C ₂ + SiC(s) \rightarrow 2SiC(s) + SiC	-42.34	-37.47
Si ₂ C ₃ + SiC(s) \rightarrow 3SiC(s) + C	-207.2	-199.4
Si ₂ C ₃ + SiC(s) \rightarrow 2SiC(s) + SiC ₂	-241.9	-240.0
Si ₃ C + SiC(s) \rightarrow 2SiC(s) + Si ₂	-96.07	-89.92
Si ₃ C ₂ + SiC(s) \rightarrow 2SiC(s) + Si ₂ C	-286.6	-284.1
Si ₃ C ₂ + SiC(s) \rightarrow 3SiC(s) + Si	-439.8	-431.3
Si ₄ C + SiC(s) \rightarrow 2SiC(s) + Si ₃	-164.9	-162.4
Si ₄ C ₂ + SiC(s) \rightarrow 2SiC(s) + Si ₃ C	-237.8	-237.0
Si ₄ C ₂ + SiC(s) \rightarrow 3SiC(s) + Si ₂	-333.9	-326.9
Si ₅ C + SiC(s) \rightarrow 2SiC(s) + Si + Si ₃	309.8	310.4

Notes. SiC(s) denotes solid SiC which is assumed to be β -SiC.

Table 3: Coefficients for calculating $\Delta G_i^0/k_B T_v$ in equation (5).

i	α_i	β_i	γ_i	δ_i	η_i	ϵ_i
1	3.11656×10^1	-1.12418×10^0	1.71784×10^2	-1.01082×10^5	1.01432×10^6	-8.78548×10^7
2	-2.96847×10^3	2.79219×10^2	5.55156×10^4	-8.91964×10^5	1.15759×10^8	-1.28618×10^{10}